Title: An Autoimmunity-associated allele of *PTPN22* enhances the innate immune response to promote protection against acute coronavirus infection

Authors: Alec M. Bevis[1], Kathryn J.L.H. Rosa[1], Nancy Schwarting[1], Tammy R. Cockerham[1], Catherine M. Kerr[1], Sunil More[2], Anthony R. Fehr[1], Robin C. Orozco[1,*]

Affiliations:

[1] Department of Molecular Biosciences, University of Kansas; Lawrence, Kansas, United States of America.

[2] Department of Veterinary Pathobiology, Oklahoma State University; Stillwater, Oklahoma, United States of America.

*Corresponding author. Email: orozco.robin@ku.edu

Abstract:

Allelic variation can impact viral clearance and disease severity, but the effect of the autoimmunity-associated allelic variant of *Ptpn22* (PEP-R619W) on antiviral immunity remains incomplete. This research defines how the loss of *Ptpn22* (PEP-null) and PEP-R619W changes antiviral immunity during acute coronavirus infection. We address the hypothesis that CRISPR/Cas9-generated PEP-null and PEP-R619W mice have enhanced antiviral immunity over PEP-WT mice during coronavirus infection. Following Mouse Hepatitis Virus (MHV) A59 infection, we interrogated pathology, cytokine production, and cellular responses in the blood, spleen, and liver of PEP-WT, PEP-null, and PEP-R619W mice. Key findings show that PEP-R619W mice have reduced viral titer and weight loss, increased survival, and more mature NK cells in the liver and spleen compared to PEP-WT mice. Interestingly, protection against disease in PEP-null mice was inoculation-dose-dependent, whereas PEP-R619W conferred immunity

regardless of infection dose. Further, Rag1-/- PEP-R619W mice had increased survival and reduced viral titer over Rag1-/- PEP-WT mice. PEP-R619W mice also had higher concentrations of IFNγ and enhanced IFNγ production by mature NK cells in the liver at 3 days post-infection. Finally, NK cell depletion elevated PEP-R619W viral titer to similar levels as PEP-WT mice. This is one of the first studies investigating the role of *Ptpn22* within NK cells and demonstrates that the *Ptpn22* allelic variant augments NK cell function and is beneficial during coronavirus infection.

One Sentence Summary:

The *Ptpn22* autoimmunity-associated allele uniquely augments innate immunity to protect against acute coronavirus infection.

Main Text:

INTRODUCTION

Allelic variation in immune-regulatory genes is associated with protective or pathogenic immune responses during disease (*1, 2*). An example is *PTPN22* and its minor 1858C>T allele (rs2476601) (*1-10*). This *PTPN22* minor allele is strongly associated with multiple autoimmune diseases, has been cited as the highest non-HLA risk allele for autoimmunity, and is present in 5-15% of North Americans (*1-10*). The generational persistence of this *PTPN22* allele, despite its strong association with various severe autoimmune diseases, poses an evolutionary paradox. A theory is that the heightened immune responses it drives, though detrimental in autoimmunity, may offer protection against infections and cancer.

44 In humans, *PTPN22* encodes for the protein Lyp, and in mice, its ortholog, PEP, is
45 predominantly expressed in immune cells (*3, 4*). The *PTPN22* 1858C>T allele results in an
46 amino acid substitution of an arginine (R) to tryptophan (W) that alters immune-regulatory
47 function in both human (Lyp-R620W) and murine ortholog (PEP-R619W) models (*3-6, 9, 11-*
48 *21*) . To better understand the function of *Ptpn22*, prior studies have frequently utilized *Ptpn22*
49 knockout (PEP-null) mice. The molecular function of PEP has been best characterized as a
50 negative regulator of T-cell receptor (TCR) and B-cell receptor (BCR) signaling, but its role in
51 other immune cells is less well understood (*3, 4, 11, 13, 16, 22-27*). Further, the Lyp-R620W and
52 PEP-R619W mutations do not directly impact phosphatase activity but lead to a loss of binding
53 capacity with other proteins, such as Csk, TRAF3, Vav, Grb2, SKAP-HOM, and NLRP3,
54 resulting in altered immune function (*3, 11-13, 17, 24*). Studies have defined several mechanisms
55 in which the *PTPN22* 1858C>T allele potentiates heightened immune responses (*3, 4, 11, 13, 16-*
56 *21, 23, 24, 28*). These same mechanisms that are detrimental during autoimmunity, such as
57 enhanced T cell function, are protective when combating chronic viral infection and cancer (*18,*
58 *19*).

59 Previous studies show that both PEP-null and PEP-R619W mice, unlike wildtype (PEP-WT)
60 mice, can clear chronic lymphocytic choriomeningitis virus clone 13 (LCMV-cl13) infection,
61 and this phenotype is attributed to their enhanced antiviral T cell effector function (*19, 29-31*).
62 However, the role of PEP and its PEP-R619W variant in virus infection has mostly been studied
63 in the context of LCMV infection and T cells (*19, 27, 29-32*). Consequently, much remains
64 unknown regarding the impact of PEP and its PEP-R619W variant on 1) innate antiviral
65 immunity, 2) non-LCMV infection models, and 3) whether PEP-null and PEP-R619W will
66 consistently exert similar immune responses during infection. Despite the comparable

67 phenotypes of PEP-null and PEP-R619W defined in LCMV-cl13 immunity, other studies have
68 highlighted several cellular and molecular differences between these two strains. For example,
69 PEP-null mice have an increased amount of Tregs, and NLRP3-mediated IL-1β production in
70 PEP-R619W myeloid cells is increased (*20, 21, 26*). These findings provide additional rationale
71 to investigate differential responses between these strains, specifically within the context of viral
72 infection. Therefore, we investigated whether PEP-null mice, PEP-R619W mice, or both can
73 modulate innate antiviral immunity to confer protection during acute coronavirus infection.

74 In this study, we investigated the impact of *Ptpn22* (PEP) and its *Ptpn22* 1858C>T allele (PEP-
75 R619W variant) on the innate immune response following acute coronavirus infection using a
76 moribund highly liver-tropic mouse hepatitis virus (MHV) strain A59. Our findings show that
77 PEP-R619W enhances natural killer (NK) cell maturation and strengthens NK effector functions,
78 and that NK cells are necessary to restrict viral replication in the liver during innate time points
79 in PEP-R619W mice. The results of this research define new mechanisms by which the
80 autoimmunity-associated allele of *PTPN22* augments innate antiviral immunity and enhances
81 protection against coronavirus infection.

82

83 **RESULTS**

84 **PEP-R619W reduces disease and viral titer during MHV A59 infection**

85 To determine the impact of *Ptpn22* and its autoimmunity-associated minor allele (PEP-R619W)
86 during acute coronavirus infection, we infected wildtype (PEP-WT) and CRISPR-Cas9
87 generated *Ptpn22* knockout (PEP-null) and PEP-R619W mice with a common murine strain of
88 coronavirus, mouse hepatitis virus (MHV) strain A59, which primarily infects the liver.
89 Following 5e4 PFU MHV A59 infection, PEP-R619W mice had significantly reduced weight

90 loss at day 5 post-infection (dpi) and 3-8 dpi during 1e5 PFU infection (Fig. 1A and 1B)
91 compared to PEP-WT mice. This was paired with significantly enhanced survival at both doses
92 compared to PEP-WT mice (Fig. 1C and 1D). At 5e4 PFU infection, PEP-null mice phenocopy
93 PEP-R619W mice. However, during 1e5 PFU infection, PEP-null mice are no longer protected
94 from MHV A59 disease and phenocopy PEP-WT mice in weight loss and survival (Fig. 1A-D).
95 We also quantified the viral load of the whole liver, as it is the primary site of replication for
96 MHV A59, at 1-, 3-, 5-, and 7- dpi via plaque assay. PEP-R619W mice had significantly reduced
97 viral titer at 1-, 3-, and 5- dpi compared to PEP-WT mice (Fig. 1E). However, PEP-null mice
98 only demonstrated reduced titer at 5 dpi (Fig. 1F). Additionally, both PEP-R619W and PEP-null
99 mice had accelerated clearance compared to PEP-WT mice, as 7/7 PEP-R619W mice and 7/8
100 PEP-null mice had cleared the infection by 7 dpi, whereas only 2/7 PEP-WT mice had cleared
101 the infection at this time point (Fig. 1E and 1F). Splenic titers showed a low level of infection at
102 1-, 3-, and 5- dpi, regardless of genotype (Fig. S1A and S1B). All mice were able to clear the
103 MHV A59 infection from the spleen by 7 dpi (Fig. S1A and S1B).

104 To determine if the reduced viral titer observed in the livers of PEP-R619W and PEP-null mice
105 (Fig. 1E and 1F) was due to PEP-driven myeloid cell-intrinsic changes in these mice, resulting in
106 decreased viral replication, we differentiated bone-marrow-derived macrophages (BMMs) and
107 bone-marrow-derived dendritic cells (BMDCs). We infected them with MHV A59 *ex vivo*, as
108 they are both readily infected *in vivo* by MHV (Fig. S1C) (*33-35*). We did not detect any
109 significant differences in viral titer across the three genotypes in either BMMs (Fig. S1D) or
110 BMDCs (Fig. S1E), indicating that PEP-R619W and PEP-null do not mediate protection by
111 directly impacting viral replication through cell-intrinsic mechanisms. Histopathologic analysis
112 of liver sections at 3 dpi following 1e5 PFU infection demonstrated multifocal regions of marked

113 hepatocellular necrosis in PEP-WT mice, characterized by infiltration of inflammatory cells and
114 deposition of edema and fibrin (black arrow) (Fig. 1G and Fig. S1F). In comparison, PEP-
115 R619W and PEP-null mice exhibited markedly reduced hepatic injury, with mild necrosis and
116 inflammation (Fig. 1G and Fig. S1F). These combined results show that PEP-R619W mice have
117 improved disease outcomes and reduced viral burden, which includes accelerated clearance,
118 during MHV A59 infection.

Fig. 1

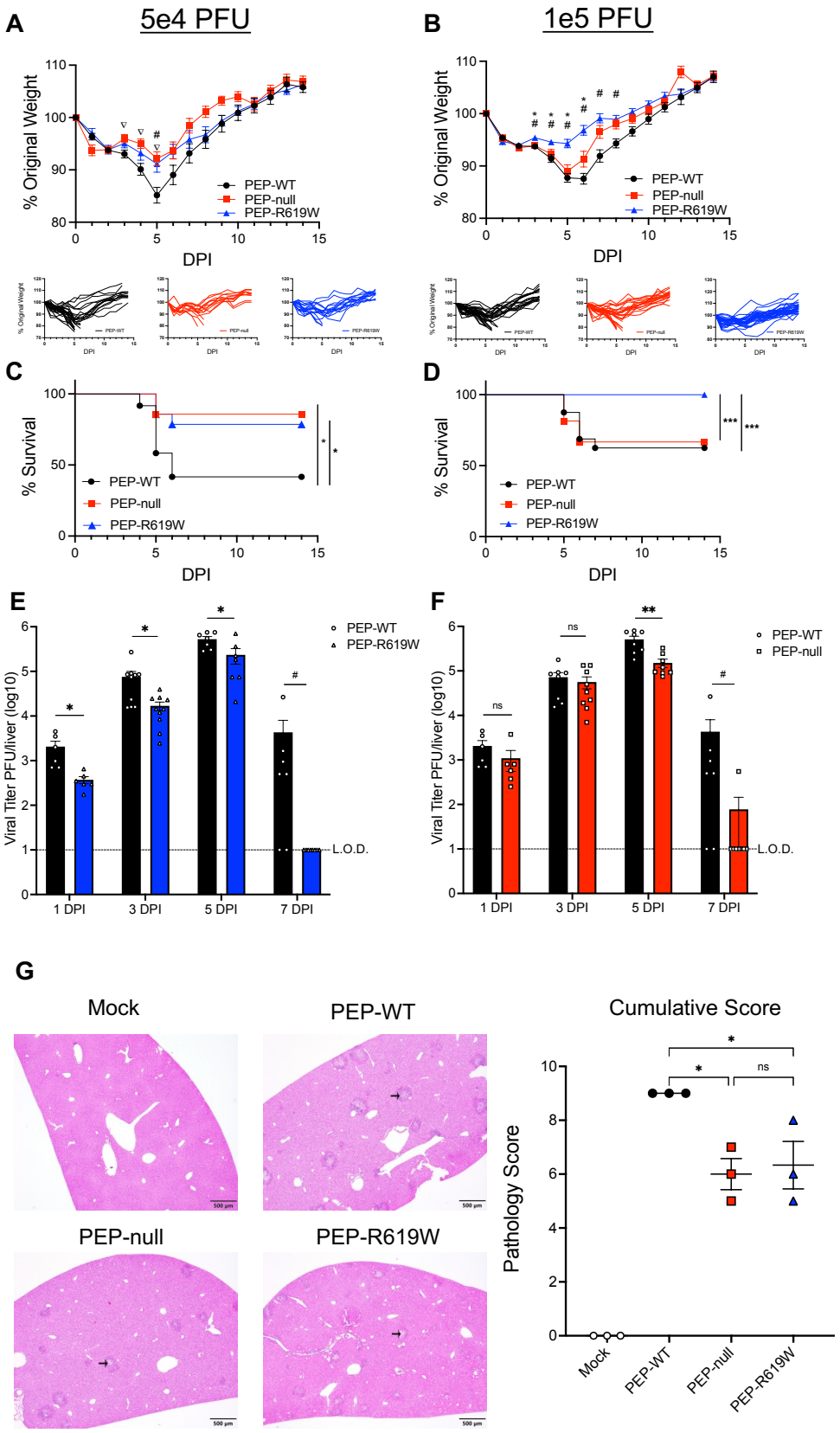
A
5e4 PFU
% Original Weight
DPI
PEP-WT
PEP-null
PEP-R619W
B
1e5 PFU
C
% Survival
D
E
Viral Titer PFU/liver (log10)
L.O.D.
1 DPI
3 DPI
5 DPI
7 DPI
F
ns
G
Mock
PEP-WT
PEP-null
PEP-R619W
Cumulative Score
Pathology Score

Figure 1: PEP-R619W mice have reduced disease during MHV A59 Infection.

C57BL/6J mice with *Ptpn22* wild type (PEP-WT, black circle), *Ptpn22* knockout (PEP-null, red square), or the *Ptpn22* autoimmune-associated allele (PEP-R619W, blue triangle), were infected with 5e4 PFU (A, C) or 1e5 PFU (B, D) MHV A59 (i.p). Mice are tracked by weight (A, B) and survival (C, D). Respective spider plots for individual mouse weights are shown below (A, B). To measure viral burden, liver homogenates from infected (5e2 PFU) PEP-WT, PEP-null, and PEP-R619W mice were used for plaque assay (E, F). Histopathology of the livers of mice at 3 dpi following 1e5 PFU MHV A59 infection, with representative photomicrographs of liver sections exhibiting areas of necrosis, inflammation, and edema/fibrin accumulation (black arrow) and cumulative pathology scores represented as mean + SEM. Scale bar = 500 µm (G). Weight loss and survival studies pooled from 3 individual experiments for each dose: Group sizes for 5e4 PFU infection (A, C) were PEP-WT n = 28, PEP-null n = 14, PEP-R619W n = 17. Group sizes for 1e5 PFU infection (B, D) were PEP-WT n = 31, PEP-null n = 27, PEP-R619W n = 31. For weight loss statistical analysis, significant p-values from One-way ANOVA with Tukey's Multiple Comparisons at each dpi are represented by #, comparing PEP-WT vs. PEP-R619W, * comparing PEP-null vs. PEP-R619W, or ∇ comparing PEP-WT vs. PEP-null. Log-rank Mantel-Cox Test (survival), *$p<0.05$, ***$p<0.001$. For whole liver titer (E, F), each symbol represents an individual mouse. The dashed line indicates the limit of detection (L.O.D.). Certain PEP-WT mice are represented in both graphs, as some experiments had all three genotypes, whereas others contained only PEP-WT vs PEP-null or PEP-R619W. Combined data from 2 independent experiments, multiple unpaired T-Tests, PEP-WT vs PEP-R619W, PEP-WT vs PEP-null, at each time point, *$p<0.01$, **$p<0.01$. 7 dpi was analyzed using Fisher's Exact Test, Cleared vs Not

142 Cleared, #$p<0.05$. For histopathological analysis, each dot represents an individual mouse, with

143 p-values from One-way ANOVA with Tukey's Multiple Comparisons shown, *$p<0.05$.

144 **PEP-R619W prolongs the survival of infected mice in the absence of T and B cells**

145 Due to the enhanced protection against disease conferred by PEP-R619W at early days post-
146 infection (Fig. 1), we wanted to determine if a strengthened innate immune response was
147 sufficient to fully protect these mice, or if T and B cells were necessary for survival during MHV
148 A59 infection. To do this, we infected Rag1-/- PEP-WT, Rag1-/- PEP-null, and Rag1-/- PEP-
149 R619W mice with 5e4 PFU or 1e5 PFU MHV A59. Like the immune-competent mice, Rag1-/-
150 PEP-R619W mice had noticeably less weight loss throughout most of the early stages of the
151 infection (Fig. 2A and 2B) and mice survived longer (Fig. 2C and 2D) compared to Rag1-/- PEP-
152 WT mice at both 5e4 and 1e5 PFU MHV A59 infection. Rag1-/- PEP-null mice also have
153 prolonged survival over Rag1-/- PEP-WT at 5e4 PFU infection (Fig. 2C). However, at 1e5 PFU
154 infection, PEP-null mice no longer had prolonged survival (Fig. 2D). These data also show that T
155 and B are necessary for overall survival, regardless of PEP- genotype or MHV A59 dose, as all
156 mice on a Rag1-/- background eventually succumb to disease (Fig. 2C and 2D). Next, we
157 measured viral load in the liver at 3- and 5-dpi. Rag1-/- PEP-R619W mice had reduced viral
158 burden compared to Rag1-/- PEP-WT mice (Fig. 2E). No difference was detected between Rag1-
159 /- PEP-WT and Rag1-/- PEP-null mice liver titers (Fig. 2F). There was no difference detected in
160 splenic viral titers at 3 and 5 dpi between Rag1-/- PEP-WT and Rag1-/- PEP-R619W mice or
161 Rag1-/- PEP-WT and Rag1-/- PEP-null mice (Fig. S2). Overall, this data suggests that PEP-null
162 enhances the innate immune response during 5e4 PFU infection in both immune competent and
163 Rag1-/- models to improve survival compared to PEP-WT mice, and these results are
164 comparable to PEP-R619W mice (Figs. 1 and 2). However, only PEP-R619W mice showed
165 enhanced protection following 1e5 PFU infection, suggesting that this autoimmune-associated

166 variant modifies the innate response through additional mechanisms compared to PEP-null, and

167 this confers increased resistance against MHV A59-associated disease (Figs. 1 and 2).

168 **Fig. 2**

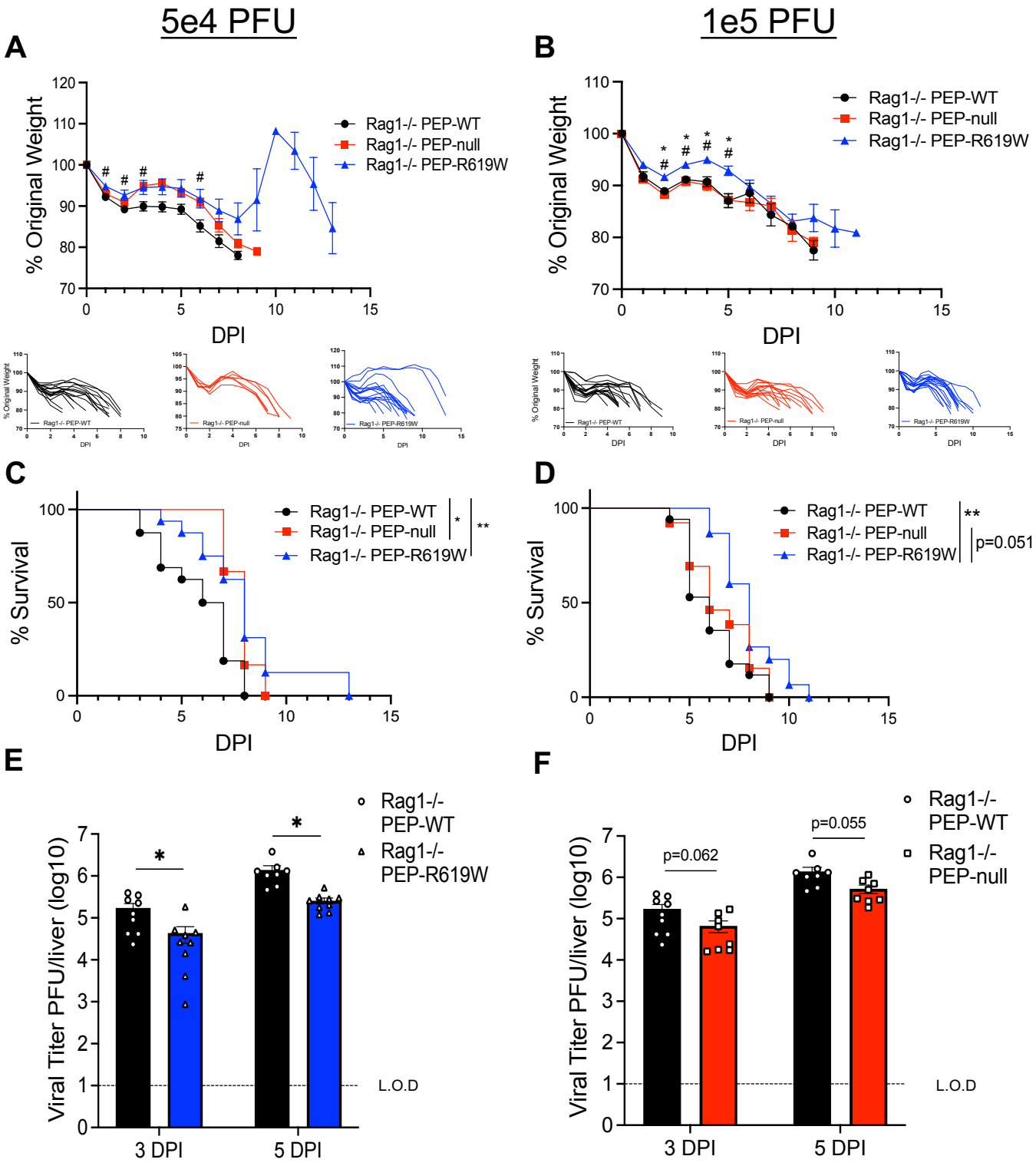
5e4 PFU
1e5 PFU
A
B
% Original Weight
DPI
Rag1-/- PEP-WT
Rag1-/- PEP-null
Rag1-/- PEP-R619W
C
D
% Survival
p=0.051
E
F
Viral Titer PFU/liver (log10)
L.O.D
3 DPI
5 DPI
p=0.062
p=0.055

Figure 2: PEP-R619W innate cells provide some protection against disease, but T and B cells are necessary for survival.

Rag1-/- PEP-WT (black circle), Rag1-/- PEP-null (red square), or Rag1-/- PEP-R619W (blue triangle), mice were infected with 5e4 PFU (A, C) or 1e5 PFU (B, D) MHV A59 (i.p), and were tracked by weight (A, B) and survival (C, D). Respective spider plots for individual mouse weights are shown below (A, B). To measure viral burden, liver homogenates from infected (5e2 PFU) Rag1-/- PEP-WT, Rag1-/- PEP-null, and Rag1-/- PEP-R619W mice were used for plaque assay (E, F). Weight loss and survival studies pooled from 2 individual experiments for each dose: Group sizes for 5e4 PFU (A, C) were Rag1-/- PEP-WT n = 16, Rag1-/- PEP-null n = 6, Rag1-/- PEP-R619W n = 16. Group sizes for 1e5 PFU (B, D) were Rag1-/- PEP-WT n = 17, Rag1-/- PEP-null n = 13, Rag1-/- PEP-R619W n = 15. For weight loss statistical analysis, significant p-values from One-way ANOVA with Tukey's Multiple Comparisons at each dpi are represented by # comparing Rag1-/- PEP-WT vs. Rag1-/- PEP-R619W and * comparing Rag1-/- PEP-null vs. Rag1-/- PEP-R619W. Log-rank Mantel-Cox Test (survival), *$p<0.05$, **$p<0.01$. For whole liver titers (E, F), each symbol represents an individual mouse. The dashed line indicates the limit of detection (L.O.D.). Certain Rag1-/- PEP-WT mice are represented in both graphs, as some experiments had all three genotypes, whereas others contained only Rag1-/- PEP-WT vs Rag1-/- PEP-null or Rag1-/- PEP-R619W. Combined data from 2 independent experiments, multiple unpaired T-Tests, Rag1-/- PEP-WT vs Rag1-/- PEP-R619W, Rag1-/- PEP-WT vs Rag1-/- PEP-null, at each time point. *$p<0.01$, **$p<0.01$.

189 **PEP-R619W mice have increased innate immune presence in the liver and spleen during**
190 **MHV A59 infection**

191 We next aimed to determine how the PEP-R619W variant augmented the innate immune
192 response. We focused on 3 dpi because, 1) this is when we can consistently observe a divergence
193 in weight loss between genotypes, 2) PEP-R619W mice have reduced liver titer and pathology at
194 this time point, and 3) this is a time point that the innate response dominates, whereas, at 5 dpi,
195 there could be some early T cell activity. As such, we investigated the innate cellular response
196 after 5e4 PFU MHV A59 infection, and similar to the observed weight loss and survival results,
197 PEP-R619W and PEP-null mice had comparable immune phenotypes at 3 dpi in the spleen (Fig.
198 S3). There was no difference detected in the bulk number of splenocytes (Fig. S3B) or frequency
199 of CD3e- CD19- (innate cells) of all live cells (Fig. S3C), regardless of infection or PEP
200 genotype. However, PEP-R619W and PEP-null mice had significantly increased frequencies of
201 NK cells and DCs compared to infected PEP-WT mice (Fig. S3D).

202 Interestingly, PEP-R619W mice had more splenic CD11b+ NK cells than PEP-WT, indicating
203 PEP-R619W NK cells are significantly more mature than PEP-WT NK cells following infection
204 (Fig. S3E) (*36, 37*). Further, there were no differences detected in the frequency of CD8α+
205 conventional dendritic cells (CD8α+ cDCs), which are likely type 1 conventional dendritic cells
206 (cDC1s) (Fig. S3F) (*38*). While the expression of activation markers CD80 and CD86 was
207 significantly upregulated post-infection in splenic CD8α+ cDCs, no significant difference was
208 detected between infected genotypes (Fig. S3G and S3H, respectively). Similar results were seen
209 in splenic CD8α- cDCs, which are likely type 2 conventional dendritic cells (cDC2s) (Fig. S3I-
210 K), though there was a decrease in CD86 expression in PEP-null and PEP-R619W splenic
211 CD8α- cDCs compared to PEP-WT post-infection (Fig. S3K) (*38*).

212 Next, we wanted to determine if, after 1e5 PFU MHV A59 infection, PEP-R619W mice had
213 enhanced antiviral immunity in the liver, as this is the main site of replication for MHV A59,
214 compared to PEP-WT and PEP-null mice. At 3 dpi, we did not detect significant differences in
215 the absolute number of liver cells (Fig. 3A) or in the frequency (%) of CD45+ cells (Fig. 3B)
216 between our mock mice (uninfected controls) and our infected PEP-WT, PEP-null, and PEP-
217 R619W mice. However, PEP-R619W mice have a higher proportion of CD3e- CD19- of CD45+
218 immune cells, which we define as an immune "innate subset," compared to PEP-WT mice (Fig.
219 3C). Delving further into this innate cell population, PEP-R619W mice had increased
220 proportions of natural killer (NK) cells, dendritic cells (DCs), and macrophages of CD45+ cells
221 over both PEP-WT and PEP-null mice (Fig. 3D). We did not detect any differences between
222 infected genotypes in plasmacytoid DCs (pDCs), monocytes, or neutrophils (Fig. 3D). We also
223 did not observe any differences in the proportion of or CD86 expression on Tim4+ macrophages,
224 which are likely Kupffer cells amongst infected PEP-WT, PEP-null, and PEP-R619W mice (Fig.
225 S4B-C) (*39-41*). Post infection, all genotypes increased CD86 expression on Tim4+
226 macrophages (Fig. S4C). Within the DC population, there was a decrease in both the frequency
227 and expression of MHC-II (Fig. S4D and S4E, respectively) in infected genotypes compared to
228 uninfected controls. Further, we did not identify any differences in the frequency and expression
229 of CD86 on DCs between infected genotypes (Fig. S4F and S4G).

230 MHV A59 infected PEP-R619W mice had more conventional NK cells compared to infected
231 PEP-WT and PEP-null mice, characterized as CD49b+ CD49a- of NK1.1+ cells, whereas the
232 inverse is considered tissue-resident type 1 innate lymphoid cells (ILC-1) (Fig. 3E) (*42, 43*).
233 Additionally, PEP-R619W conventional NK cells were more mature (CD11b+) compared to
234 PEP-WT (Fig. 3F), and overall, PEP-R619W mice had more mature conventional NK cells

235 (CD11b+ CD49b+ CD49a- NK1.1+) compared to both PEP-WT and PEP-null mice during
236 coronavirus infection (Fig. 3G). These mature NK cells are of particular interest because, as NK
237 cells mature, they enhance their effector function potential, including increased interferon-
238 gamma (IFNγ) production and elevated expression of cytotoxic molecules, such as perforin and
239 granzyme B (*36, 37*). Collectively, these data demonstrate that the PEP-R619W variant enhances
240 both splenic and liver innate antiviral immunity, specifically increasing the overall amount and
241 maturity of NK cells.

242 **Fig. 3**

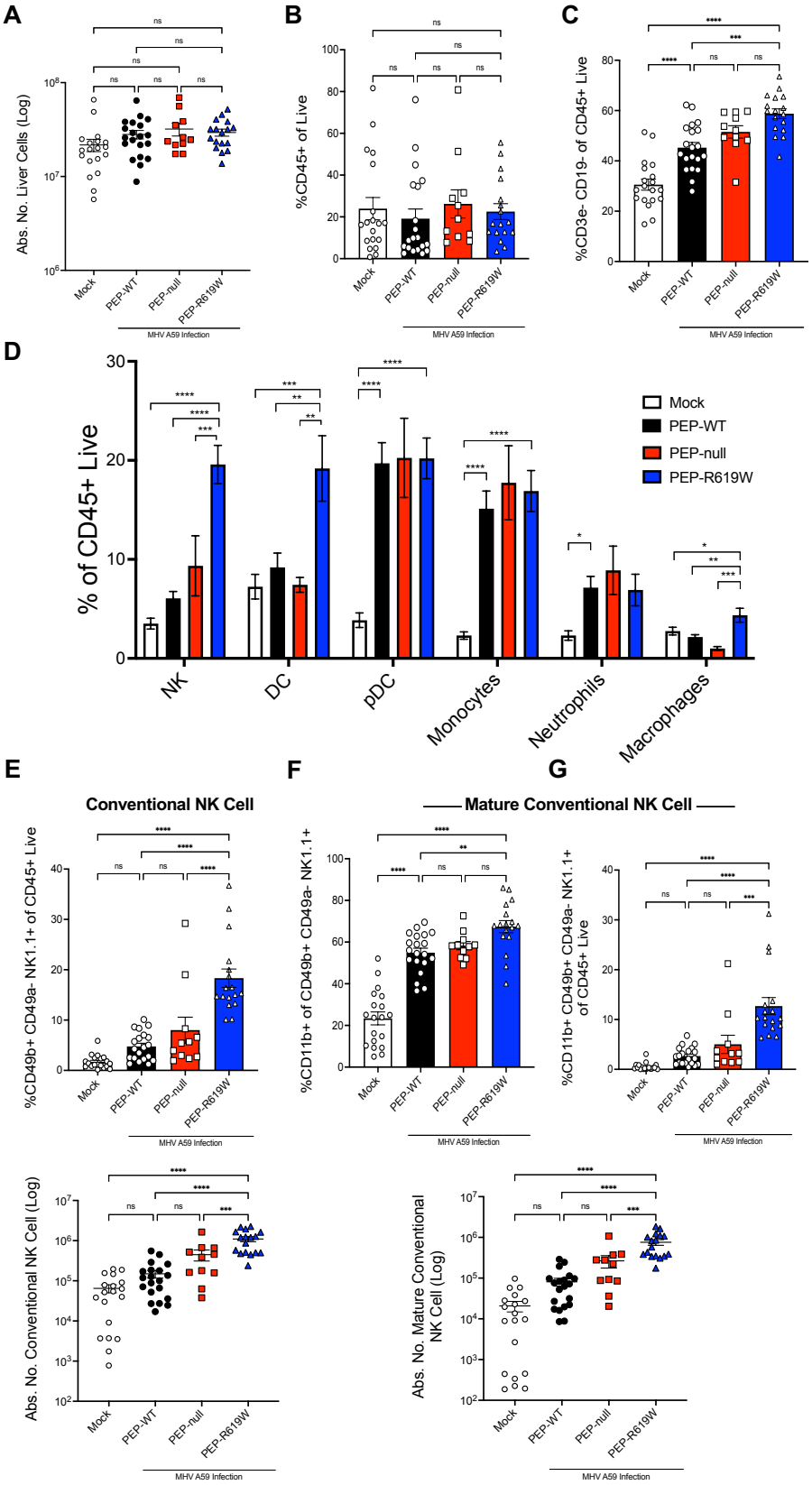
A
Abs. No. Liver Cells (Log)
B
%CD45+ of Live
C
%CD3e- CD19- of CD45+ Live
Mock
PEP-WT
PEP-null
PEP-R619W
MHV A59 Infection
D
% of CD45+ Live
Mock
PEP-WT
PEP-null
PEP-R619W
NK
DC
pDC
Monocytes
Neutrophils
Macrophages
E
Conventional NK Cell
%CD49b+ CD49a- NK1.1+ of CD45+ Live
F
Mature Conventional NK Cell
%CD11b+ of CD49b+ CD49a- NK1.1+
G
%CD11b+ CD49b+ CD49a- NK1.1+ of CD45+ Live
Abs. No. Conventional NK Cell (Log)
Abs. No. Mature Conventional NK Cell (Log)

Figure 3: PEP-R619W mice have more innate immune and mature NK cells in the Liver.

Following PBS injection (Mock, white bar, circle) or 1e5 PFU MHV A59 infection (i.p) in PEP-WT (black bar, circle), PEP-null (red bar, square), and PEP-R619W (blue bar, triangle) mice, at 3 dpi the liver was perfused, harvested, and antibody stained for flow cytometric analysis. The absolute count of liver cells for all genotypes (A). Frequencies (%) of CD45+ cells of live cells (B) and of CD3e- CD19- of CD45+ Live (C). Frequency (%) of several innate cells of CD45+ cells is shown (D). Gating strategy for all innate subsets is: Lymphocytes> Single cell x2> autofluorescent-> Live> CD45+> CD3e- CD19-> Ly6G- Ly6C+/- (non-neutrophils). NK Cells: innate subsets> NK1.1+. DCs: innate subsets> NK1.1-> CD11c+ PDCA-1-. pDCs: innate subsets> NK1.1-> PDCA-1+ CD11c+/-. Monocytes: innate subsets> NK1.1-> Ly6C^{hi} CD11b+. Macrophage: innate subsets> NK1.1-> Ly6C- CD11b+/-> F4/80+ CD11b+. Neutrophils: Lymphocytes> Single cell x2> autofluorescent-> Live> CD3e- CD19-> Ly6G+ Ly6C+. Frequency (%) conventional NK cells of CD45+ (E). Frequency (%) mature conventional NK cells (F) of CD45+ cells (G). Gating strategy for NK subsets: Conventional NK Cells: innate subsets> NK1.1+> CD49b+ CD49a-. Mature Conventional NK Cells: Conventional NK Cells> CD11b+. Quantification of flow cytometric data was pooled from 6 independent experiments. Each symbol represents an individual mouse. Mock mice are a mixture of all 3 genotypes. p-values from One-way ANOVA with Tukey's Multiple Comparisons are shown for each panel. *$p<0.05$, **$p<0.01$, ***$p<0.001$, ****$p<0.0001$.

262 **PEP-null splenic mature NK cell effector functions are changed depending on the MHV**
263 **A59 inoculation dose**

264 Since our data showed that PEP-R619W mice have significantly more mature NK cells in both
265 the liver and spleen at 3 dpi, we next wanted to determine if the NK cells amongst our mice had
266 changed functional properties. Again, we observed inoculation dose-dependent differences,
267 where at 5e4 PFU, PEP-null and PEP-R619W mice had similar NK cell immune phenotypes in
268 the spleen (Fig. S5A-F). Specifically, following 5e4 PFU infection, PEP-null and PEP-R619W
269 mature splenic NK cells had less CD107a, a marker of degranulation (Fig. S5A and S5B),
270 increased perforin (Fig. S5C and S5D), and no detectable difference in IFNγ (Fig. S5E and S5F)
271 compared to PEP-WT mature splenic NK cells. Yet at 1e5 PFU, PEP-null and PEP-WT
272 phenotypes were more similar in the spleen (Fig. S5G-L). With 1e5 PFU infection, PEP-R619W
273 mature splenic NK cells had reduced degranulation marker CD107a (Fig. S5G and S5H),
274 increased perforin (Fig. S5I and S5J), and an increase in frequency, but not expression, of IFNγ
275 (Fig. S5K and S5L) compared to PEP-WT and PEP-null mature splenic NK cells. This data
276 provides some insight into why PEP-null mice have differing phenotypes (survival) during
277 different doses of MHV A59 infection, as differential immune activation at 1e5 PFU infection
278 may be responsible for the previously described increase in morbidity (Figs. 1 and 2).

279 **PEP-R619W enhances liver mature NK cell effector function and the overall production of**
280 **IFNγ during virus infection**

281 As only PEP-R619W mice, but not PEP-null, had more mature conventional NK (M-cNK) cells
282 compared to PEP-WT mice at 3 dpi in the liver, we next investigated if PEP-R619W M-cNK
283 cells have altered effector functions compared to PEP-WT M-cNK cells. Following 1e5 PFU
284 infection, at 3 dpi in the liver, PEP-R619W M-cNK cells (CD11b+ CD49b+ CD49a- NK1.1+)

285 have higher expression of (i) IFNγ, (ii) T-bet, (iii) granzyme B, and (iv) perforin, compared to
286 PEP-WT M-cNK cells (Fig. 4A, i-iv). There was no difference detected in the expression of (v)
287 TNFα or (vi) CD107a between PEP-WT and PEP-R619W M-cNK cells (Fig. 4A, v-vi). Further,
288 PEP-R619W M-cNK cells were more poly-functional compared to PEP-WT, as there was an
289 increased proportion of IFNγ+ Perforin+ and IFNγ+ Perforin+ TNFα+ M-cNK cells in PEP-
290 R619W mice.

291 Next, we examined the magnitude of the cytokine/chemokine response both systemically and in
292 the whole liver at 3 dpi. Strikingly, out of the thirteen different cytokines and chemokines
293 paneled in the serum (Fig. 4C), only the concentration of IFNγ was significantly increased in
294 PEP-R619W mice (Fig. 4D), yet all other molecules, including interferon-alpha (IFNα) (Fig.
295 4E), which is necessary for protection against MHV A59 infection, were unchanged between
296 infected genotypes (*44*). Similar results were detected in the whole liver homogenate (Fig. 4F-
297 H). To corroborate these findings, we measured the levels of IFNβ in the liver at 3 dpi in our
298 PEP-WT, PEP-null, and PEP-R619W mice. We detected no difference between infected
299 genotypes (Fig. 4I).

300 Given the enhanced M-cNK IFNγ expression and the overall increased IFNγ concentration in our
301 PEP-R619W mice, we next wanted to determine if IFNγ and/or IFNγ-signaling was necessary
302 for survival and weight retention during MHV A59 infection. To test this, we infected WT, IFNγ
303 knockout (IFNγ KO), and IFNγ receptor knockout (IFNγR KO) mice with 5e4 PFU of MHV
304 A59. Both IFNγ KO and IFNγR KO mice had more severe weight loss (Fig. 4J) and nearly 100%
305 mortality (Fig. 4K) compared to WT mice, demonstrating the importance of IFNγ for protection
306 during MHV A59 infection.

307 Taken together, these data show that PEP-R619W liver M-cNK cells produce more IFNγ and are
308 more poly-functional than PEP-WT M-cNK cells, contributing to the increased levels of IFNγ in
309 both the serum and liver at 3 dpi. Further, IFNγ and IFNγ signaling are critical for survival. This
310 suggests that the protection conferred by PEP-R619W during MHV A59 infection may be
311 driven, in part, by enhanced NK cell IFNγ production.

Fig. 4

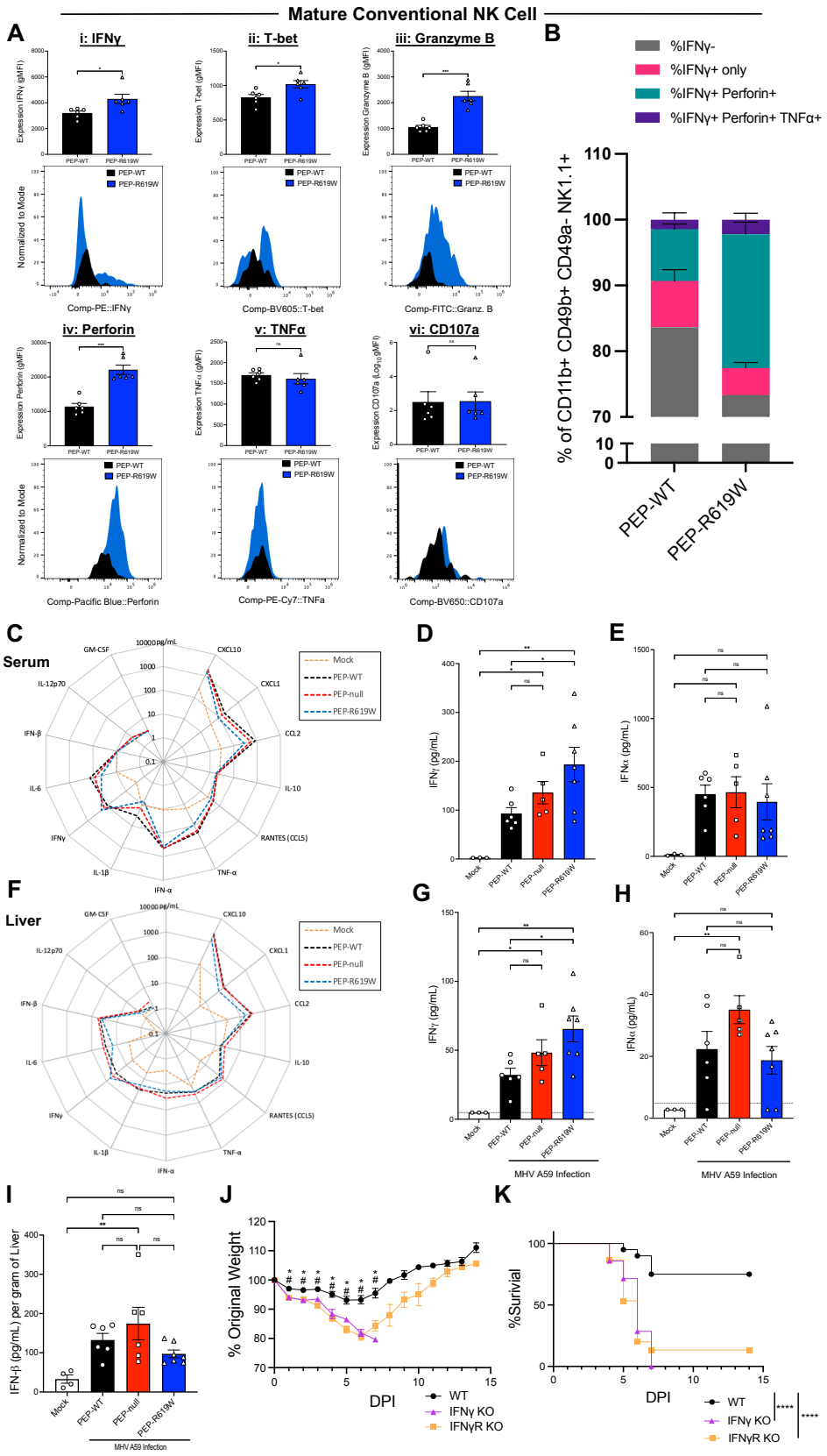
Mature Conventional NK Cell
A
i: IFNγ
ii: T-bet
iii: Granzyme B
iv: Perforin
v: TNFα
vi: CD107a
PEP-WT
PEP-R619W
Comp-PE::IFNγ
Comp-BV605::T-bet
Comp-FITC::Granz. B
Comp-Pacific Blue::Perforin
Comp-PE-Cy7::TNFa
Comp-BV650::CD107a
B
%IFNγ-
%IFNγ+ only
%IFNγ+ Perforin+
%IFNγ+ Perforin+ TNFα+
% of CD11b+ CD49b+ CD49a- NK1.1+
C
Serum
D
E
F
Liver
G
H
Mock
PEP-null
MHV A59 Infection
I
IFN-β (pg/mL) per gram of Liver
J
% Original Weight
DPI
WT
IFNγ KO
IFNγR KO
K
%Survival

313 **Figure 4: PEP-R619W augments mature conventional NK antiviral functions during**
314 **coronavirus infection.**
315 3 dpi liver M-cNK analysis following 1e5 PFU MHV A59 infection (i.p) in PEP-WT (black bar,
316 circle) and PEP-R619W (blue bar, triangle) mice. Expression (gMFI) of IFNγ (i), T-bet (ii),
317 Granzyme B (iii), Perforin (iv), TNFα (v), and CD107a (vi) in Mature Conventional NK cells,
318 with representative histograms below (A). Proportion of IFNγ- (grey), IFNγ+ only (pink), IFNγ+
319 Perforin+ (teal), and IFNγ+ Perforin+ TNFα+ (purple) of Mature Conventional NK Cells (B).
320 Expression of 13 different cytokines and chemokines were quantified using LEGENDplex.
321 Radar plots showing the 13 different cytokines from the serum (C) and liver (F), with select
322 cytokines, IFNγ (D, G) and IFNα (E, H), quantified to the right. IFNβ concentration in the liver
323 at 3 dpi [ELISA] (I). C57BL/6 mice with wild type (PEP-WT, black circle), IFNγ knockout
324 (IFNγ KO, purple triangle), or IFNγ Receptor knockout (IFNγR KO, orange square) were
325 infected with 5e4 PFU MHV A59 (i.p). Mice are tracked by weight (J) and survival (K).
326 Quantification of flow cytometric data is representative of 3 independent experiments. p-values
327 from Welch's unpaired t test are shown, *$p<0.05$, **$p<0.01$, ***$p<0.001$. LEGENDplex assays
328 are from 1 experiment. Each symbol represents an individual mouse. Mock mice are a mixture of
329 all 3 genotypes. p-values from One-way ANOVA with Tukey's Multiple Comparisons are shown
330 for each panel. *$p<0.05$, **$p<0.01$, ***$p<0.001$. Weight loss and survival studies pooled from 2
331 individual experiments. Group sizes were PEP-WT n = 19, IFNγ KO n = 4, and IFNγR KO n =
332 15. For weight loss statistical analysis, significant p-values from One-way ANOVA with Tukey's
333 Multiple Comparisons at each dpi are represented by # comparing PEP-WT vs. IFNγ KO, or *
334 PEP-WT vs. IFNγR KO. Log-rank Mantel-Cox Test (survival), ****$p<0.0001$.

335 **NK Cell maturation is accelerated in PEP-null and PEP-R619W mice**

336 Due to the increased presence of mature NK cells in the spleens (CD11b+ of NK1.1+) and liver
337 (CD11b+ of CD49b+ CD49a- NK1.1+) of PEP-R619W mice post-infection (Fig. S3E, Fig. 3E-
338 G), we examined if PEP-R619W NK cells had differential maturation states compared to PEP-
339 WT at homeostasis. Previous studies have shown that murine NK cells follow a four-stage
340 developmental program, defined by the subsequent acquisition and loss of surface receptors
341 CD27 and CD11b, and these maturation states can be seen in the spleen (*36, 37*). The four
342 stages, from least to most mature, are defined as; (i) CD27- CD11b- (Double Negative, DN), (ii)
343 CD27+ CD11b-, (iii) CD27+ CD11b+ (Double Positive, DP), and (iv) CD27- CD11b+ (*36, 37*).
344 This developmental program is associated with the stepwise acquisition of NK cell effector
345 function, and the accumulation of terminally mature NK cells (CD27- CD11b+) plateaus at 8
346 weeks of age (*36, 37*). At 5 weeks of age, PEP-null and PEP-R619W splenic NK cells had
347 differential maturation states compared to PEP-WT (Fig. 5). Specifically, of the NK cell
348 repertoire, PEP-WT mice had more DP NK cells, but PEP-null and PEP-R619W had increased
349 proportions of terminally mature (CD27- CD11b+) NK cells at 5 weeks of age (Fig. 5A, 5D, 5E).
350 However, at 8 weeks of age, there were no differences detected in the proportion of DP or
351 terminally mature NK cells between the three genotypes of mice. Collectively, this data indicates
352 that PEP may negatively impact NK cell maturation at homeostasis, which could play a role in
353 the observed differences in mature NK cell presence and function in PEP-R619W mice
354 following MHV A59 infection.

355 **Fig. 5**

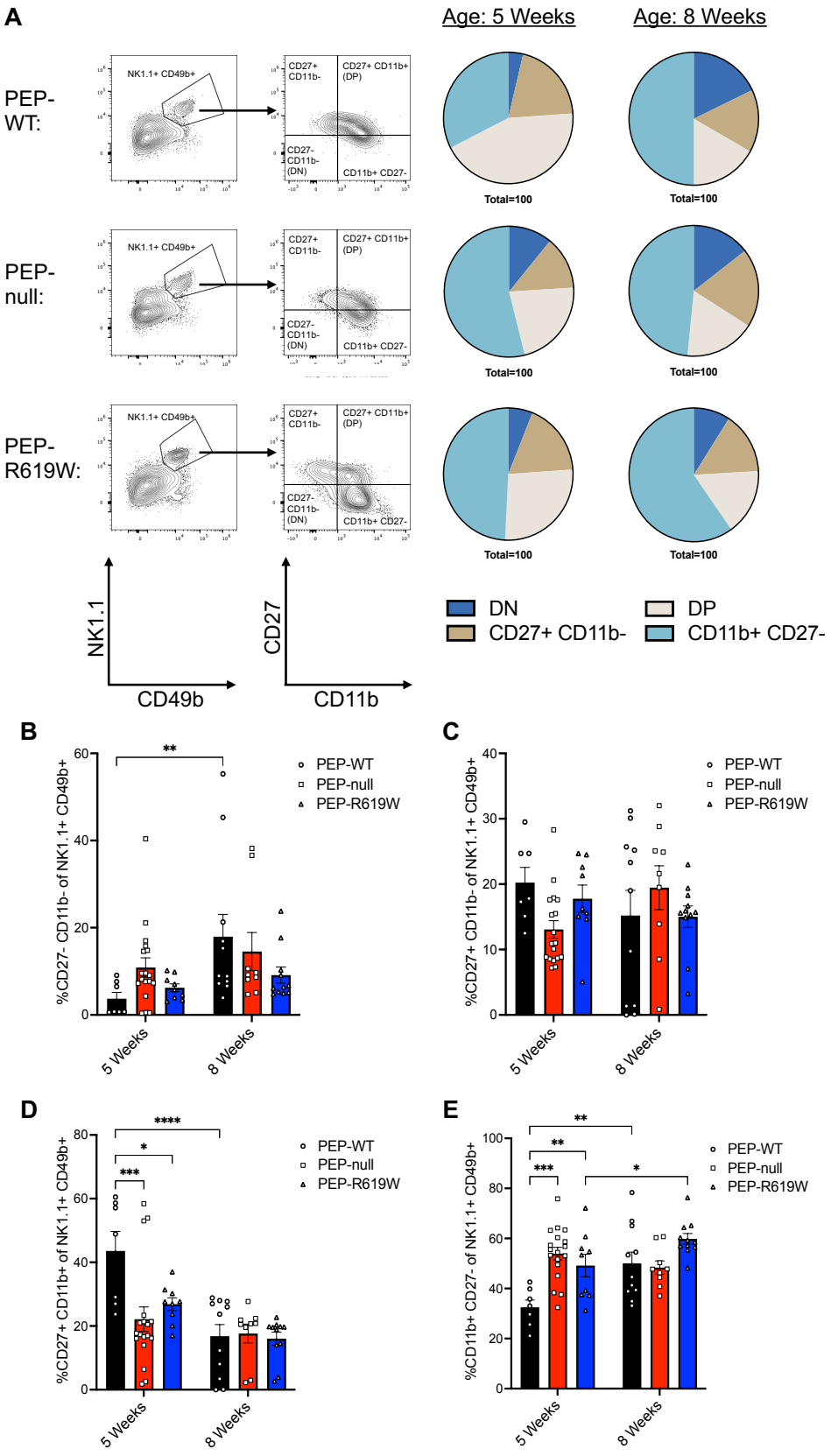
A
Age: 5 Weeks
Age: 8 Weeks
PEP-WT:
PEP-null:
PEP-R619W:
NK1.1+ CD49b+
CD27+ CD11b-
CD27+ CD11b+ (DP)
CD27- CD11b- (DN)
CD11b+ CD27-
Total=100
NK1.1
CD49b
CD27
CD11b
DN
DP
CD27+ CD11b-
CD11b+ CD27-
B
%CD27- CD11b- of NK1.1+ CD49b+
PEP-WT
PEP-null
PEP-R619W
5 Weeks
8 Weeks
C
%CD27+ CD11b- of NK1.1+ CD49b+
D
%CD27+ CD11b+ of NK1.1+ CD49b+
E
%CD11b+ CD27- of NK1.1+ CD49b+

356 **Figure 5: PEP-null and PEP-R619W splenic NK cell repertoires have higher proportions of**
357 **terminally mature NK cells at 5 weeks of age.**
358 Whole spleens were harvested and stained for flow cytometric analysis from 5-week-old or 8-
359 week-old mice as indicated. Representative flow plots from 5-week-old mice are shown from
360 CD3e- CD19- populations, pie charts represent the proportion of the NK1.1+ CD49b+
361 population that are: CD27- CD11b- (double negative, DN), CD27+ CD11b-, CD27+ CD11b+
362 (double positive, DP), or CD11b+ CD27- (A). Quantification for frequency (%) of CD27-
363 CD11b- (double negative, DN) (B), CD27+ CD11b- (C), CD27+ CD11b+ (double positive, DP)
364 (D), or CD11b+ CD27- (E) NK cells (NK1.1+ CD49b+). Gating strategy for examined NK cells:
365 Lymphocytes> Single cell x2> autofluorescent-> Live> CD3e- CD19-> NK1.1+ CD49b+>
366 CD27+/- CD11b+/-. Frequencies of flow cytometric data are combined from 5 independent
367 experiments. Each symbol represents an individual mouse. p-values from Two-way ANOVA
368 with Tukey's Multiple Comparisons are shown for each panel. *$p<0.05$, **$p<0.01$, ***$p<0.001$,
369 ****$p<0.0001$.

370 **PEP-R619W NK cells restrict viral replication and enhance IFNγ production during**
371 **coronavirus infection**
372 Given our observation that NK cells are more mature and functional, and there are more of them
373 in PEP-R619W mice during infection, we next wanted to determine if NK cells were necessary
374 for driving disease protection during MHV A59 infection. To test this, we administered an anti-
375 NK1.1 (α-NK1.1) depleting antibody (clone PK136) or anti-IgG isotype control (α-Iso) two days
376 before MHV A59 infection. Subsequent injections were administered every four days after the
377 initial treatment (Fig. 6A). NK depletion was verified at all key time points, both within the
378 spleen and in the peripheral blood (Fig. S6A-E). Loss of NK cells in PEP-R619W mice resulted
379 in a decreased capacity to control virus infection, as viral burden in the liver at 3- and 5- dpi rose
380 to comparable levels of both α-NK1.1 PEP-WT and isotype-treated PEP-WT mice (Fig. 6B). In
381 addition, isotype-treated PEP-R619W mice maintained the reduced levels of viral titer in the
382 liver compared to isotype-treated PEP-WT mice at these time points (Fig. 6B). These data
383 indicate that PEP-R619W NK cells effectively reduce liver viral load, but PEP-WT NK cells
384 have minimal impact on combating viral replication within the liver. We again detected no
385 differences in the splenic titers, regardless of the presence of NK cells (Fig. S6F). This data
386 suggests that in PEP-R619W mice, the increased presence of NK cells in the liver is one of the
387 key innate cells responsible for combating viral replication during the early days of infection.
388 Our data support this conclusion, as all NK-sufficient PEP-R619W mice, including immune-
389 competent (Fig. 1E), Rag1-/- (Fig. 2E), and α-Iso (Fig. 6B) mice, had significantly reduced liver
390 viral titers at days 3 and 5 post-infection compared to PEP-WT counterpart mice. In contrast, this
391 protection was lost in α-NK1.1 PEP-R619W mice (Fig. 6B). Next, we wanted to determine if NK
392 cells were a critical source of IFNγ in our PEP-R619W mice. Upon depletion of NK cells, the

393 levels of IFNγ in liver homogenate at 3 dpi in α-NK1.1 PEP-R619W mice were significantly
394 reduced compared to α-Iso PEP-R619W mice (Fig. 6C). Further, α-Iso PEP-R619W had a
395 significantly higher concentration of IFNγ compared to α-Iso PEP-WT, recapitulating the
396 cytokine profiling data previously shown (Fig. 4G). In conclusion, this data highlights that PEP-
397 R619W enhances NK cell function to protect against MHV A59 viral replication in the liver
398 through, in part, boosting the production of NK cell-derived IFNγ.

399 **PEP-R619W NK cells do not mediate weight loss, survival, or liver histopathology during**
400 **coronavirus infection**

401 Since PEP-R619W NK cells mediate viral titer at early days post-infection and are a key source
402 of IFNγ, we next wanted to determine if they were necessary for mediating weight loss and
403 survival during MHV A59 infection. Following 1e5 PFU MHV A59 infection, NK cell depletion
404 in either PEP-WT or PEP-R619W mice did not result in changes in weight loss, survival, or in
405 liver histopathology compared to NK-sufficient PEP-WT and PEP-R619W counterparts (Fig.
406 6D-F and Fig. S6G).

407 Overall, this data indicates that NK cells in PEP-R619W mice play a specific role in combating
408 MHV A59 infection by restricting viral replication and are critical producers of IFNγ within the
409 primary site of replication, the liver. However, these NK cells are dispensable for protection
410 against weight loss, survival, and liver damage. While NK cell depletion in PEP-R619W mice
411 increased viral load and reduced liver IFNγ concentration, the same depletion in PEP-WT mice
412 did not affect liver viral titer or IFNγ production. This disparity can potentially be attributed to
413 the reduced number and impaired function of M-cNK cells in the livers of PEP-WT mice at 3 dpi
414 (Fig. 3D-G, Fig. 4A and 4B), making their absence less impactful on viral replication.

415 **Fig. 6**

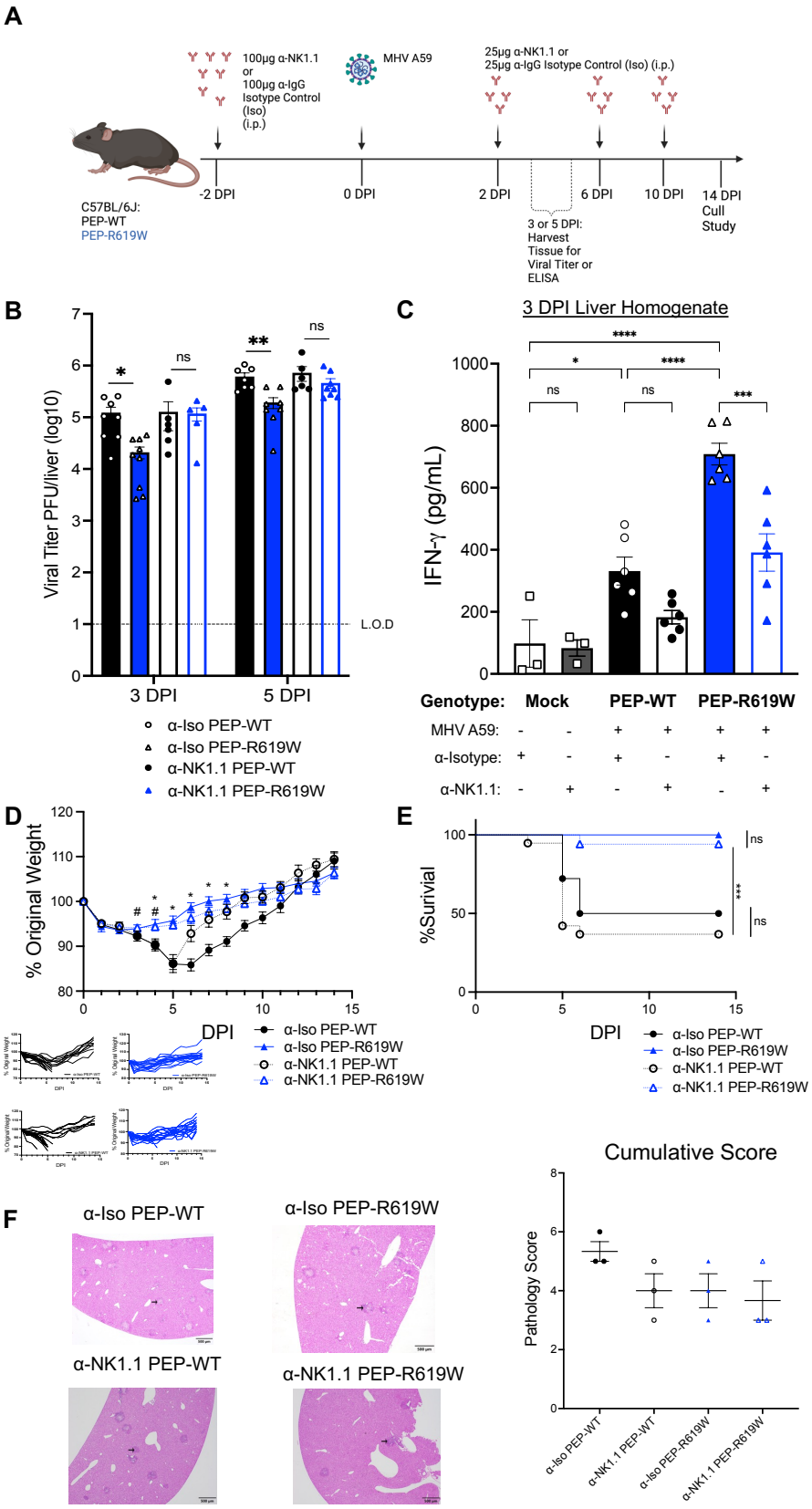
A
100µg α-NK1.1 or 100µg α-IgG Isotype Control (Iso) (i.p.)
MHV A59
25µg α-NK1.1 or 25µg α-IgG Isotype Control (Iso) (i.p.)
C57BL/6J: PEP-WT PEP-R619W
-2 DPI
0 DPI
2 DPI
6 DPI
10 DPI
14 DPI Cull Study
3 or 5 DPI: Harvest Tissue for Viral Titer or ELISA
B
Viral Titer PFU/liver (log10)
L.O.D
3 DPI
5 DPI
α-Iso PEP-WT
α-Iso PEP-R619W
α-NK1.1 PEP-WT
α-NK1.1 PEP-R619W
C
3 DPI Liver Homogenate
IFN-γ (pg/mL)
Genotype: Mock PEP-WT PEP-R619W
MHV A59:
α-Isotype:
α-NK1.1:
D
% Original Weight
DPI
E
%Surivial
DPI
F
α-Iso PEP-WT
α-Iso PEP-R619W
α-NK1.1 PEP-WT
α-NK1.1 PEP-R619W
Cumulative Score
Pathology Score

416 **Figure 6: PEP-R619W NK Cells control viral burden and are key producers of IFNγ**
417 **during MHV A59 infection.**
418 PEP-WT and PEP-R619W mice received Natural Killer cell depleting antibody (α-NK1.1, Clone
419 PK136) or non-depleting isotype control antibody (α-Iso) as indicated prior- and post-MHV A59
420 infection (i.p) (A). Following 5e2 PFU MHV A59 infection in α-Iso PEP-WT (black, black
421 circle), α-Iso PEP-R619W (blue, blue triangle), α-NK1.1 PEP-WT (clear, black circle) and α-
422 NK1.1 PEP-R619W (clear, blue triangle) mice, the whole liver was harvested at the indicated
423 dpi, homogenized, and viral titer was quantified via Plaque Assay (B). Mice were infected with
424 1e5 PFU MHV A59 infection (i.p), and at 3 dpi, the whole liver was harvested, homogenized,
425 and the levels of IFNγ were determined by ELISA (C). Following 1e5 PFU MHV A59 infection,
426 mice were tracked by weight (D) and survival (E). Respective spider plots for individual mouse
427 weights are shown below (D). Histopathology of the livers of mice at 3 dpi following 1e5 PFU
428 MHV A59 infection, with representative photomicrographs of liver sections exhibiting areas of
429 necrosis, inflammation, and edema/fibrin accumulation (black arrow) and cumulative pathology
430 scores represented as mean + SEM. Scale bar = 500 μm (F). Each symbol represents an
431 individual mouse for whole liver titer (B) and IFNγ ELISA (C). Viral titers are pooled data from
432 2 independent experiments at each time point, comparisons are shown from multiple unpaired T-
433 Tests, α-Iso PEP-WT vs α-Iso PEP-R619W, α-NK1.1 PEP-WT vs α-NK1.1 PEP-R619W,
434 *$p<0.01$, **$p<0.01$. The dashed line indicates the limit of detection (L.O.D.). IFNγ ELISA is
435 representative of two independent experiments, p-values from One-way ANOVA with Tukey's
436 Multiple Comparisons are shown, *$p<0.05$, **$p<0.01$, ***$p<0.001$, ****$p<0.0001$. Mock mice
437 are a mixture of both genotypes. Weight loss and survival studies were pooled from 2 individual
438 experiments. Group sizes were α-Iso PEP-WT n = 18, α-Iso PEP-R619W n = 17, α-NK1.1 PEP-

439 WT n = 19, and α-NK1.1 PEP-R619W n = 17. For weight loss statistical analysis (D), significant
440 p-values from One-way ANOVA with Tukey's Multiple Comparisons at each dpi are represented
441 by # comparing α-NK1.1 PEP-WT vs α-NK1.1 PEP-R619W, or * comparing α-Iso PEP-WT vs.
442 α-Iso PEP-R619W. Log-rank Mantel-Cox Test (survival) (E), ***$p<0.001$. For histopathological
443 analysis, each dot represents an individual mouse, with p-values from One-way ANOVA with
444 Tukey's Multiple Comparisons shown, *$p<0.05$.

445 **DISCUSSION**

446 Despite the strong genetic link between the minor allele of *PTPN22* and the development of
447 various autoimmune diseases, this allele persists in the human population. A potential theory lies
448 in the fact that the mechanisms driving heightened immune responses, while pathogenic in the
449 context of autoimmunity, are likely protective when defending against infections and cancer.
450 Previous studies support this reasoning, as PEP-R619W mice exhibit enhanced antiviral
451 immunity during chronic LCMV-cl13 infection and increased antitumor immunity, resulting in
452 reduced disease severity compared to PEP-WT mice (*18, 19*). Similar results in PEP-null mice
453 have been reported during LCMV-cl13 infection (*29-31*). However, these diseases are chronic.
454 Thus, we were interested in determining if PEP-null and/or PEP-R619W mice would also have
455 improved disease outcomes during acute, moribund coronavirus infection, MHV A59.

456 Our results show that PEP-R619W and PEP-null do not always phenocopy each other.
457 Regardless of whether PEP-null mice were fully immune-competent or on a Rag1-/- genetic
458 background, their phenotypes were comparable to PEP-R619W mice after 5e4 PFU infection,
459 but demonstrated increased susceptibility following 1e5 PFU infection and mirrored the
460 outcomes observed in PEP-WT mice (Figs. 1 and 2). Despite similar splenic innate profiles and
461 NK activation between PEP-null and PEP-R619W mice at 3 dpi following 5e4 PFU infection,
462 after 1e5 PFU MHV A59 infection, PEP-null splenic NK cell phenotypes were comparable to
463 PEP-WT (Fig. S3 and S5). These findings add to the current literature, highlighting that there are
464 differences between PEP-null and PEP-R619W. While PEP-null and PEP-R619W mice may be
465 similar in certain scenarios, such as in LCMV-cl13 antiviral immunity, there are other examples
466 where they can differ (*19-21, 27, 29-31*). This may lie in cellular and/or molecular differences
467 between these strains. For example, previous studies show that PEP-null mice have more Tregs

468 than PEP-WT and PEP-R619W mice, and that the PEP-R619W mutation does not directly
469 impact phosphatase activity (*3, 4, 9, 23, 24, 26-28*). Instead, the mutation disrupts molecular
470 interactions with other proteins, such as TRAF3 and Csk, leading to altered immune function (*3,*
471 *4, 9, 23, 24, 26-28*). The precise ways in which established molecular interactions and other
472 potential mechanisms that influence innate immune cell function diverge between PEP-null and
473 PEP-R619W mice are poorly understood. Further investigation into these mechanisms would
474 provide crucial insight into the varying outcomes observed between these strains during MHV
475 A59 infection.

476 Our data shows that PEP-R619W protects against murine coronavirus, MHV A59, associated
477 disease (Fig. 1). This is paired with reduced liver viral titer at early days post-infection, and
478 accelerated clearance compared to PEP-WT mice (Fig. 1). This protection in PEP-R619W mice
479 was partially mediated by an enhanced innate immune response. This is further strengthened by
480 the results of our studies using Rag1-/- models, as Rag1-/- PEP-R619W mice had reduced
481 disease compared to Rag1-/- PEP-WT mice (Fig. 2). These data indicate that PEP-R619W
482 differentially modulates the innate immune response to defend against acute MHV A59 infection
483 (Figs. 1 and 2). This data is further supported by the immune phenotyping of both the spleen and
484 liver at 3 dpi, where PEP-R619W mice had more innate immune cells compared to PEP-WT
485 mice (Fig. 3, Fig. S3 and S4).

486 We interrogated the immune response in the liver following 1e5 PFU infection to define how
487 PEP-R619W uniquely enhanced innate antiviral immunity. Notably, PEP-R619W mice had more
488 NK cells, DCs, and macrophages compared to PEP-WT and PEP-null mice (Fig. 3D). However,
489 we detected no differences in type-I interferon (IFN-I) production, which is necessary for
490 survival following MHV A59 infection (*44*). There were no changes in the pDC population,

491 which are critical producers of IFN-I (Fig. 3D), or in the systemic and liver homogenate levels of
492 IFNα and IFNβ (Fig. 4C, E, F, H, and I) between infected genotypes, indicating that PEP-
493 R619W protects through alternative mechanisms, such as enhancing NK cell function. NK cells
494 can directly lyse infected cells through the release of perforin and granzyme B, are the primary
495 producers of IFNγ during the innate immune response, and these functions are enhanced as NK
496 cells mature (*36, 37, 45, 46*). These effector functions are necessary for combating murine
497 cytomegalovirus (MCMV) disease and viral replication and have been specifically shown to be
498 vital in driving the innate immune response in the liver post-infection (*47-51*). As such, we more
499 closely interrogated the NK cell compartment in PEP-WT and PEP-R619W mice post-MHV
500 A59 infection.

501 We investigated the role of NK cells during MHV A59 infection and discovered that: 1) there
502 were more mature conventional NK (M-cNK) cells in the spleen and liver of PEP-R619W mice
503 (Fig. 3D-G and Fig. S3D, S3E), 2) PEP-R619W enhanced M-cNK effector function and
504 polyfunctionality compared to PEP-WT (Fig. 4A and 4B), and 3) PEP-R619W NK cells, but not
505 PEP-WT NK cells, are necessary for restricting viral replication in the liver at 3 and 5 dpi (Fig.
506 6B) and are a critical source of IFNγ (Fig. 6C). Taken together, these results indicate that PEP-
507 R619W augments M-cNK cell antiviral function in the liver during MHV A59 infection, leading
508 to reduced viral replication, but PEP-R619W M-cNK cells do not directly mediate weight loss,
509 survival, or liver pathology (Fig. 6D-F). These findings add to recent work and highlight the
510 protective role of NK cells at the primary site of coronavirus infection, as NK cells are critical
511 for combating SARS-CoV-2 replication in both human and non-human primate lungs (*52-54*).
512 However, our data also demonstrates that viral burden and disease symptoms are not always
513 directly correlated, and this is supported by other viral infection models. An example of this is

514 seen in chronic LCMV-cl13 infection, where weight loss is driven by CD8 T-cell
515 immunopathology (*55*).

516 We are one of the first groups to investigate the function of PEP in NK cells, yet the molecular
517 role of PEP in NK cells remains undefined, despite being the immune cells with the highest
518 Lyp/PEP expression in humans and mice (*56, 57*). Our results show that at 5 weeks of age, PEP-
519 R619W mice have more mature NK cells post-MHV A59 infection at 3 dpi in the spleen and
520 liver compared to PEP-WT (Fig. S3 and Fig. 3). This phenotype persists at homeostasis, where
521 both PEP-null and PEP-R619W mice had a higher proportion of terminally mature (CD11b+
522 CD27-) NK cells in the spleen compared to PEP-WT counterparts (Fig. 5). Despite these
523 findings, the molecular functions of PEP within NK cells, and how the PEP-R619W variant
524 accelerates maturity and enhances effector functions during infection, remains unknown. These
525 results warrant additional studies defining the molecular mechanisms by which PEP and PEP-
526 R619W regulate NK cell maturity and function at homeostasis and during disease.

527 In conclusion, our results indicate that the autoimmunity-associated allele of *PTPN22* enhances
528 innate antiviral immunity against acute murine coronavirus infection, MHV A59, and adds to the
529 growing literature supporting the protective role of this allele during viral and tumorigenic
530 challenges (*18, 19*). We have shown a divergence in protection against MHV A59 infection in
531 PEP-null mice in an inoculation dose-dependent manner, whereas PEP-R619W was protective
532 regardless of infection dose. Additionally, we showed that PEP-R619W boosts innate cell
533 infiltration, enhances NK cell maturation and function, and, overall, reduces disease following
534 murine coronavirus infection. This data highlights that PEP-R619W uniquely modifies immune
535 function through distinct mechanisms compared to both PEP-WT and PEP-null, especially in NK
536 cells. These findings provide further rationale for testing the protective capacity of PEP-R619W

537 in additional infection models and defining how PEP-R619W augments immunity in a context-
538 dependent manner.

539 **MATERIALS AND METHODS**

540 **Study design**

541 The primary objective of this study was to define how the loss of *Ptpn22* (PEP-null) and its
542 autoimmunity-associated allelic variant (PEP-R619W) impacts antiviral immune responses
543 during an acute coronavirus infection, MHV A59. Following MHV A59 infection, we assessed
544 the ability of MHV A59 to cause disease in our PEP-WT, PEP-null, and PEP-R619W mice. This
545 was achieved by measuring several different markers of pathogenesis (weight loss, survival, viral
546 titer, and histology), performing in-depth immune phenotyping in the spleen and liver (flow
547 cytometry), quantifying cytokine production (Legendplex), and testing if NK cells were
548 necessary for viral control and disease progression (NK depletion). Sample sizes were
549 determined based on prior experiments, and the number of independent experiments and
550 replicates was described in the figure legends. For most experiments, randomization and blinding
551 were not used as the results involved objective readouts. For liver histopathology, the manuscript
552 data were not shared, and the sample genotypes were blinded until the analysis was completed.

553 **Ethics Statement**

554 The University of Kansas (KU) Institutional Animal Care and Use Committee (IACUC)
555 reviewed and approved all animal studies under protocol number AUS 278-01.

556 **Mice**

557 Both male and female mice at 5 weeks of age were used in all studies unless otherwise noted.
558 We do not observe sex-based differences in these studies. C57BL/6J mice and C57BL/6 Rag1-/-

559 mice were originally purchased from Jackson Labs and then bred and maintained in the
560 University of Kansas Animal Care Unit (ACU) facilities. *Ptpn22* knockout (PEP-null) and
561 *Ptpn22* R619W (PEP-R619W) mice were generated using CRISPR/Cas9 technology using
562 methods previously reported (*15, 18, 19*) (*58*). PEP-null Rag1-/- and PEP-R619W Rag1-/- mice
563 were derived as previously described (*18*). IFNγ KO (RRID: IMSR_JAX:002287) and IFNγR
564 KO (RRID: IMSR_JAX:003288) mice were purchased from Jackson Labs and were housed and
565 maintained in the University of Kansas ACU facilities as detailed above.

566 **Cell Culture**

567 <u>HeLa-MHVR and 17Cl-1 Cells:</u>

568 HeLa cells expressing the MHV receptor CEACAM1a (HeLa-MHVR) were cultured in
569 Advanced Dulbecco's modified Eagle's medium (DMEM) supplemented with 10% FBS, 1% L-
570 glutamine, and 1% Penicillin/Streptomycin, and 17Cl-1 cells were grown in DMEM
571 supplemented with 5% FBS, 5% Tryptose Phosphate Broth, and 2% Penicillin/Streptomycin (*59*)
572 (*60*).

573 <u>Bone Marrow Dendritic Cells (BMDC) and Macrophages (BMM):</u>

574 To generate BMDCs, bone marrow cells were isolated from PEP-WT, PEP-null, and PEP-
575 R619W mouse femurs. Following isolation, cells were cultured in Advanced DMEM
576 supplemented with 10% FBS, 1% L-glutamine, 1% Penicillin/Streptomycin, and 100ng/mL
577 FLT3L (Stem Cell Technologies, Vancouver, CA). For BMMs, bone marrow cells were isolated
578 and cultured in Roswell Park Memorial Institute medium (RPMI) supplemented with 10% FBS,
579 1% L-glutamine, and 1% Penicillin/Streptomycin with 50ng/mL M-CSF (Stem Cell
580 Technologies, Vancouver, CA) for 8 days. An additional 10 mL of M-CSF-containing media was

581 added to BMM cultures on day 3 (*61*), and on day 8, differentiated cells were harvested, counted,
582 and replated for further assays.

583 **MHV A59 Production, Titer, and Infections**

584 MHV A59 stocks were grown in 17Cl-1 cells, and viral titers were determined on HeLa cells
585 expressing the MHV receptor CEACAM1a (HeLa-MHVR), as previously described (*59, 60, 62-*
586 *64*). Briefly, HeLa-MHVRs were seeded in 12-well plates the day before infection. The
587 following day, once the HeLa-MHVRs were grown to 90-95% confluency, 10-fold dilutions of
588 titer samples were prepared, and the HeLa-MHVRs were inoculated for a 45-to-60-minute
589 adsorption phase, followed by 1 mL overlay per well of 1:1 mixture of 1.2% Agarose and 2x
590 DMEM (10% FBS, 1% L-Gln, 1% Pen/Strep). Once solidified, 500 µL D2 media (DMEM, 2%
591 FBS, 1% L-Gln, 1% Pen/Strep) was added to the overlay. The plaques were counted and
592 recorded 48 hours later for viral titer (PFU/sample) calculation.

593 For *in vivo* infections, mice were inoculated with 500 PFU, 5e4 PFU, or 1e5 PFU MHV A59 in a
594 final volume of 200 µL sterile PBS via intraperitoneal (i.p.) injection. Throughout all infections,
595 mice were weighed daily and euthanized if weight loss was greater than 20% of the original
596 starting weight. To determine viral load, the whole liver and spleen were harvested and
597 homogenized in 5 mL or 1 mL sterile DMEM, respectively, centrifuged to remove cellular
598 debris, and stored at -80^{0}C. The viral titer was determined on HeLa-MHVR cells as detailed
599 above.

600 For *ex vivo* Bone Marrow Dendritic Cell (BMDC) and Bone Marrow Macrophage (BMM)
601 infections, cells were inoculated at a multiplicity of infection (MOI) of 0.1 with a 45-to-60-
602 minute adsorption phase. The viral inoculum was aspirated, and 1 mL of advanced DMEM
603 supplemented with 10% FBS, 1% L-glutamine, 1% Penicillin/Streptomycin or RPMI

604 supplemented with 10% FBS, 1% L-glutamine, and 1% Penicillin/Streptomycin, for BMDC or
605 BMM, respectively, was added per well and incubated for 24 hours. At 24 hours post-infection,
606 the cells were scraped and resuspended before being placed in the -80^{0}C freezer overnight.
607 Following freeze-thaw, the virus from the supernatant and cells was combined and tittered on
608 HeLa-MHVRs as described above.

609 **Leukocyte Isolation and Flow Cytometry**

610 Mice were euthanized at indicated time points in line with AVMA and KU IACUC guidelines by
611 CO2 inhalation followed by cervical dislocation before tissue harvest.

612 The spleen was excised at indicated days post-infection, smashed over 40 µm filters, rinsed with
613 DMEM, and centrifuged to remove debris. The cell pellet was resuspended in 2 mL ACK red
614 cell lysis buffer, incubated at RT for 2 minutes, quenched with 10 mL DMEM, and centrifuged.
615 The resultant pellet was resuspended in 2 mL advanced DMEM supplemented with 10% FBS,
616 1% L-glutamine, 1% Penicillin/Streptomycin to generate a single cell suspension.

617 Whole livers were harvested following cardiac perfusion with 15-20 mL sterile PBS and placed
618 in 3 mL DMEM supplemented with 10% FBS on ice. Livers were digested and processed using a
619 murine liver dissociation kit (Miltenyi Biotec, Bergisch Gladbach, North Rhine-Westphalia,
620 Germany) per the manufacturer's protocol. Following centrifugation, the cell pellet was
621 resuspended in 1 mL sterile DMEM (1% L-glutamine), gently overlaid onto a 20 mL 33%
622 percoll gradient in PBS, and centrifuged at 800xg for 25 minutes at room temperature (RT) (*65*).
623 After aspiration, the cell pellet was resuspended in 2 mL Advanced DMEM (supplemented with
624 10% FBS, 1% L-glutamine, 1% Penicillin/Streptomycin) to generate a single cell suspension.

625 To harvest peripheral blood for NK Depletion verification, 50 µL of blood was acquired via
626 retro-orbital (r.o.) bleeds using heparinized capillary tubes. 10 µL of blood was plated in a 96-
627 well plate for each sample. 100 µL of ACK red cell lysis buffer was added and incubated at RT
628 for 2 minutes, quenched with 100 µL Advanced DMEM (supplemented with 10% FBS, 1% L-
629 glutamine, 1% Penicillin/Streptomycin), centrifuged, and resuspended in 200 µL of media to
630 generate a single cell suspension.

631 All single cell suspensions were counted using Vi-CELL BLU (Beckman Coulter, Brea, CA).
632 The concentration of each sample was adjusted to plate 2e6 cells/well in round-bottom 96-well
633 plates for antibody staining and flow cytometric analysis.

634 All flow cytometry was performed on the Cytek Aurora 5 laser system (355 nm [UV], 405 nm
635 [Vio], 488 nm [Blue], 561 nm [YG], and 640 nm [Red]) spectral flow cytometer (Fremont, CA,
636 US). Single stain control Biolegend Compensation Beads were used for unmixing (San Diego,
637 California, U.S). Unmixed files were analyzed using FlowJo Software (BD Biosciences, San
638 Diego, California). Antibodies used in varying combinations (depending upon the experiment)
639 are shown below in the Supplementary Materials (Table S1).

640 All samples were incubated with diluted Fc block (Biolegend) for 10 minutes and then stained
641 for 30 minutes at 4^0C in the dark for surface marker staining in serum-free PBS. For intracellular
642 cytokine staining, cells were incubated with brefeldin A (BFA, Thermo Scientific) for four hours
643 at 37^0C before surface staining. BD Cytofix and Permwash kit or Tonbo Foxp3 Fix/Perm kit
644 were used according to manufacturers' protocols for intracellular cytokine or intranuclear
645 transcription factor staining, respectively.

646

647 **Cytokine and Chemokine Quantification**

648 500 µL of blood was acquired via retro-orbital (r.o.) bleeds using non-heparinized capillary tubes
649 before euthanasia. After incubating at RT for 30 minutes, the blood was centrifuged at 13,000
650 RPM for 10 minutes at RT, and the serum supernatant was collected and stored at -80^{0}C for
651 future analysis. As described above, the whole liver was homogenized in 5 mL DMEM,
652 centrifuged to remove cellular debris, and stored at -80^{0}C for future analysis. Serum and liver
653 homogenate antiviral cytokines and chemokines were quantified using a LEGENDplex assay
654 (Biolegend), with the serum being diluted 1:2 as described in the manufacturer protocol. In a
655 separate experiment, a portion of the left lateral liver lobe was harvested, weighed, homogenized,
656 and the concentration of IFNβ was determined using the Mouse IFN-Beta ELISA Kit (PBL
657 Assay Science). The levels of IFNγ were determined using LEGEND MAX™ Mouse IFNγ
658 ELISA Kit (Biolegend) in NK cell depletion experiments following whole liver harvest and
659 homogenization at indicated time points.

660 **Natural Killer (NK) cell depletion**

661 Depletion of NK cells was achieved through i.p. injection of 100 µg anti-NK1.1 monoclonal
662 antibodies (clone PK136) two days before infection and followed by 25 µg anti-NK1.1 injections
663 every four days to sustain depletion (Bio-X-Cell). In parallel, separate mice were administered
664 control IgG injections at the same dosage and timings as detailed above (Bio-X-Cell). The
665 experimental outline is shown in Supplementary Figure 6.

666 **Histopathology**

667 Whole livers were harvested following cardiac perfusion with 15-20 mL sterile PBS, followed by
668 10-15 mL of 4% PFA diluted in PBS, and placed in 20 mL of 10% PFA diluted in PBS

669 (minimum ratio of 1 gram tissue:10 mL 10% PFA). After 72 hours at 4^0C in the dark, a
670 representative section from each lateral and medial (right and left) lobe was cut and processed
671 for routine hematoxylin and eosin (H&E) staining. The liver lesions were blindly scored by an
672 American College of Veterinary Pathology Board-certified pathologist. The lesions scored were
673 inflammation, necrosis, and edema/fibrin on a scale of 0–10% (score 1), 10–40% (score 2), 40–
674 70% (score 3), and >70% (score 4). Cumulative scores were obtained for each mouse and
675 presented as total pathology score.

676 **Statistical Analysis and Graphing**

677 All graphs and appropriate statistical analysis for data were done in GraphPad Prism (La Jolla,
678 CA). The type of statistical tests used are listed in each figure legend. Data was considered
679 statistically significant if the p-value<0.05. Data with a p-value>0.05 was determined non-
680 significant, and pairwise comparisons were either not labeled or represented with "ns." Figure
681 legends indicate if data are from pooled experiments or are representative of multiple studies.
682 Most graphs display mean + SEM, unless otherwise stated.

683

684 **Supplementary Materials**

685

686 Figure S1: PEP-R619W does not impact splenic titer or restrict viral replication in myeloid cells.
687 Figure S2: Splenic titers are unchanged in Rag1-/- mice regardless of PEP genotype.
688 Figure S3: PEP-R619W increases the splenic innate immune population.
689 Figure S4: Representative gating strategy for different liver immune cell populations and
690 additional quantification of immune cells.

691 Figure S5: Infection dose-dependent impact on splenic mature NK function.

692 Figure S6: NK depletion protocol and NK-depleted spleen titer and histopathology scores.

693 Table S1: Flow Cytometry Antibodies

694 # REFERENCES

695

696 1. P. K. Gregersen, B. Diamond, R. M. Plenge, GWAS implicates a role for quantitative
697 immune traits and threshold effects in risk for human autoimmune disorders. *Curr Opin*
698 *Immunol* **24**, 538-543 (2012).
699 2. R. J. Xavier, J. D. Rioux, Genome-wide association studies: a new window into immune-
700 mediated diseases. *Nat Rev Immunol* **8**, 631-643 (2008).
701 3. L. H. Armitage, M. A. Wallet, C. E. Mathews, Influence of PTPN22 Allotypes on Innate
702 and Adaptive Immune Function in Health and Disease. *Front Immunol* **12**, 636618
703 (2021).
704 4. N. Bottini, E. J. Peterson, Tyrosine phosphatase PTPN22: multifunctional regulator of
705 immune signaling, development, and disease. *Annu Rev Immunol* **32**, 83-119 (2014).
706 5. N. Bottini, T. Vang, F. Cucca, T. Mustelin, Role of PTPN22 in type 1 diabetes and other
707 autoimmune diseases. *Semin Immunol* **18**, 207-213 (2006).
708 6. G. L. Burn, L. Svensson, C. Sanchez-Blanco, M. Saini, A. P. Cope, Why is PTPN22 a
709 good candidate susceptibility gene for autoimmune disease? *FEBS Lett* **585**, 3689-3698
710 (2011).
711 7. R. C. Chiaroni-Clarke *et al.*, The association of PTPN22 rs2476601 with juvenile
712 idiopathic arthritis is specific to females. *Genes Immun* **16**, 495-498 (2015).
713 8. L. M. Gomez *et al.*, PTPN22 C1858T polymorphism in Colombian patients with
714 autoimmune diseases. *Genes Immun* **6**, 628-631 (2005).
715 9. L. B. Ivashkiv, PTPN22 in autoimmunity: different cell and different way. *Immunity* **39**,
716 91-93 (2013).
717 10. H. Wang *et al.*, Identification of PTPN22, ST6GAL1 and JAZF1 as psoriasis risk genes
718 demonstrates shared pathogenesis between psoriasis and diabetes. *Exp Dermatol* **26**,
719 1112-1117 (2017).
720 11. H. H. Chang *et al.*, PTPN22 modulates macrophage polarization and susceptibility to
721 dextran sulfate sodium-induced colitis. *J Immunol* **191**, 2134-2143 (2013).
722 12. X. Dai *et al.*, A disease-associated PTPN22 variant promotes systemic autoimmunity in
723 murine models. *J Clin Invest* **123**, 2024-2036 (2013).
724 13. Y. Wang *et al.*, The autoimmunity-associated gene PTPN22 potentiates toll-like receptor-
725 driven, type 1 interferon-dependent immunity. *Immunity* **39**, 111-122 (2013).
726 14. Y. Wang *et al.*, PTPN22 Variant R620W Is Associated With Reduced Toll-like Receptor
727 7-Induced Type I Interferon in Systemic Lupus Erythematosus. *Arthritis Rheumatol* **67**,
728 2403-2414 (2015).
729 15. X. Lin *et al.*, CRISPR-Cas9-Mediated Modification of the NOD Mouse Genome With
730 Ptpn22R619W Mutation Increases Autoimmune Diabetes. *Diabetes* **65**, 2134-2138
731 (2016).
732 16. A. M. Wallis *et al.*, TRAF3 enhances TCR signaling by regulating the inhibitors Csk and
733 PTPN22. *Sci Rep* **7**, 2081 (2017).
734 17. E. Fiorillo *et al.*, Autoimmune-associated PTPN22 R620W variation reduces
735 phosphorylation of lymphoid phosphatase on an inhibitory tyrosine residue. *J Biol Chem*
736 **285**, 26506-26518 (2010).
737 18. R. C. Orozco, K. Marquardt, K. Mowen, L. A. Sherman, Proautoimmune Allele of
738 Tyrosine Phosphatase, PTPN22, Enhances Tumor Immunity. *J Immunol* **207**, 1662-1671
739 (2021).

740 19. R. C. Orozco *et al.*, Autoimmunity-associated allele of tyrosine phosphatase gene
741 PTPN22 enhances anti-viral immunity. *PLoS Pathog* **20**, e1012095 (2024).
742 20. M. R. Spalinger *et al.*, NLRP3 tyrosine phosphorylation is controlled by protein tyrosine
743 phosphatase PTPN22. *J Clin Invest* **126**, 1783-1800 (2016).
744 21. M. R. Spalinger *et al.*, PTPN22 regulates NLRP3-mediated IL1B secretion in an
745 autophagy-dependent manner. *Autophagy* **13**, 1590-1601 (2017).
746 22. K. Hasegawa *et al.*, PEST domain-enriched tyrosine phosphatase (PEP) regulation of
747 effector/memory T cells. *Science* **303**, 685-689 (2004).
748 23. T. Vang *et al.*, LYP inhibits T-cell activation when dissociated from CSK. *Nat Chem Biol*
749 **8**, 437-446 (2012).
750 24. E. L. Hornick, A. M. Wallis, G. A. Bishop, TRAF3 enhances type I interferon receptor
751 signaling in T cells by modulating the phosphatase PTPN22. *Sci Signal* **15**, eabn5507
752 (2022).
753 25. A. Gjorloff-Wingren, M. Saxena, S. Williams, D. Hammi, T. Mustelin, Characterization
754 of TCR-induced receptor-proximal signaling events negatively regulated by the protein
755 tyrosine phosphatase PEP. *Eur J Immunol* **29**, 3845-3854 (1999).
756 26. C. J. Maine *et al.*, PTPN22 alters the development of regulatory T cells in the thymus. *J*
757 *Immunol* **188**, 5267-5275 (2012).
758 27. C. J. Maine, K. Marquardt, J. Cheung, L. A. Sherman, PTPN22 controls the germinal
759 center by influencing the numbers and activity of T follicular helper cells. *J Immunol*
760 **192**, 1415-1424 (2014).
761 28. T. Vang *et al.*, Autoimmune-associated lymphoid tyrosine phosphatase is a gain-of-
762 function variant. *Nat Genet* **37**, 1317-1319 (2005).
763 29. C. J. Maine, J. R. Teijaro, K. Marquardt, L. A. Sherman, PTPN22 contributes to
764 exhaustion of T lymphocytes during chronic viral infection. *Proc Natl Acad Sci U S A*
765 **113**, E7231-E7239 (2016).
766 30. T. Jofra *et al.*, Protein tyrosine phosphatase PTPN22 has dual roles in promoting
767 pathogen versus homeostatic-driven CD8 T-cell responses. *Immunol Cell Biol* **95**, 121-
768 128 (2017).
769 31. T. Jofra *et al.*, Extrinsic Protein Tyrosine Phosphatase Non-Receptor 22 Signals
770 Contribute to CD8 T Cell Exhaustion and Promote Persistence of Chronic Lymphocytic
771 Choriomeningitis Virus Infection. *Front Immunol* **8**, 811 (2017).
772 32. X. Zhou, S. Ramachandran, M. Mann, D. L. Popkin, Role of lymphocytic
773 choriomeningitis virus (LCMV) in understanding viral immunology: past, present and
774 future. *Viruses* **4**, 2650-2669 (2012).
775 33. B. C. Turner, E. M. Hemmila, N. Beauchemin, K. V. Holmes, Receptor-dependent
776 coronavirus infection of dendritic cells. *J Virol* **78**, 5486-5490 (2004).
777 34. O. L. Wijburg, M. H. Heemskerk, C. J. Boog, N. Van Rooijen, Role of spleen
778 macrophages in innate and acquired immune responses against mouse hepatitis virus
779 strain A59. *Immunology* **92**, 252-258 (1997).
780 35. H. Zhou, S. Perlman, Preferential infection of mature dendritic cells by the JHM strain of
781 mouse hepatitis virus. *Adv Exp Med Biol* **581**, 411-414 (2006).
782 36. S. Kim *et al.*, In vivo developmental stages in murine natural killer cell maturation. *Nat*
783 *Immunol* **3**, 523-528 (2002).
784 37. L. Chiossone *et al.*, Maturation of mouse NK cells is a 4-stage developmental program.
785 *Blood* **113**, 5488-5496 (2009).

786 38. D. Vremec, J. Pooley, H. Hochrein, L. Wu, K. Shortman, CD4 and CD8 expression by
787 dendritic cell subtypes in mouse thymus and spleen. *J Immunol* **164**, 2978-2986 (2000).
788 39. H. Wu *et al.*, TIM-4 interference in Kupffer cells against CCL4-induced liver fibrosis by
789 mediating Akt1/Mitophagy signalling pathway. *Cell Prolif* **53**, e12731 (2020).
790 40. M. Ni *et al.*, T-Cell Immunoglobulin and Mucin Domain-Containing Protein-4 Is Critical
791 for Kupffer Cell Homeostatic Function in the Activation and Resolution of Liver
792 Ischemia Reperfusion Injury. *Hepatology* **74**, 2118-2132 (2021).
793 41. W. Li, Y. Yang, L. Yang, N. Chang, L. Li, Monocyte-derived Kupffer cells dominate in
794 the Kupffer cell pool during liver injury. *Cell Rep* **42**, 113164 (2023).
795 42. P. D. Krueger *et al.*, Murine liver-resident group 1 innate lymphoid cells regulate optimal
796 priming of anti-viral CD8+ T cells. *J Leukoc Biol* **101**, 329-338 (2017).
797 43. D. K. Sojka *et al.*, Tissue-resident natural killer (NK) cells are cell lineages distinct from
798 thymic and conventional splenic NK cells. *Elife* **3**, e01659 (2014).
799 44. L. Cervantes-Barragan *et al.*, Control of coronavirus infection through plasmacytoid
800 dendritic-cell-derived type I interferon. *Blood* **109**, 1131-1137 (2007).
801 45. N. K. Bjorkstrom, B. Strunz, H. G. Ljunggren, Natural killer cells in antiviral immunity.
802 *Nat Rev Immunol* **22**, 112-123 (2022).
803 46. S. N. Waggoner *et al.*, Roles of natural killer cells in antiviral immunity. *Curr Opin Virol*
804 **16**, 15-23 (2016).
805 47. T. P. Salazar-Mather, J. S. Orange, C. A. Biron, Early murine cytomegalovirus (MCMV)
806 infection induces liver natural killer (NK) cell inflammation and protection through
807 macrophage inflammatory protein 1alpha (MIP-1alpha)-dependent pathways. *J Exp Med*
808 **187**, 1-14 (1998).
809 48. T. P. Salazar-Mather, T. A. Hamilton, C. A. Biron, A chemokine-to-cytokine-to-
810 chemokine cascade critical in antiviral defense. *J Clin Invest* **105**, 985-993 (2000).
811 49. K. A. Daniels *et al.*, Murine cytomegalovirus is regulated by a discrete subset of natural
812 killer cells reactive with monoclonal antibody to Ly49H. *J Exp Med* **194**, 29-44 (2001).
813 50. A. O. Dokun *et al.*, Specific and nonspecific NK cell activation during virus infection.
814 *Nat Immunol* **2**, 951-956 (2001).
815 51. J. Loh, D. T. Chu, A. K. O'Guin, W. M. Yokoyama, H. W. t. Virgin, Natural killer cells
816 utilize both perforin and gamma interferon to regulate murine cytomegalovirus infection
817 in the spleen and liver. *J Virol* **79**, 661-667 (2005).
818 52. H. Balachandran *et al.*, NK cells modulate in vivo control of SARS-CoV-2 replication
819 and suppression of lung damage. *PLoS Pathog* **20**, e1012439 (2024).
820 53. C. A. Fielding *et al.*, SARS-CoV-2 host-shutoff impacts innate NK cell functions, but
821 antibody-dependent NK activity is strongly activated through non-spike antibodies. *Elife*
822 **11**, (2022).
823 54. C. van Eeden, L. Khan, M. S. Osman, J. W. Cohen Tervaert, Natural Killer Cell
824 Dysfunction and Its Role in COVID-19. *Int J Mol Sci* **21**, (2020).
825 55. H. Baazim *et al.*, CD8(+) T cells induce cachexia during chronic viral infection. *Nat*
826 *Immunol* **20**, 701-710 (2019).
827 56. K. Douroudis, A. Shcherbakova, H. Everaus, A. Aints, PTPN22 gene regulates natural
828 killer cell proliferation during in vitro expansion. *Tissue Antigens* **76**, 315-318 (2010).
829 57. BioGPS. vol. 2025.
830 58. S. Pelletier, S. Gingras, D. R. Green, Mouse genome engineering via CRISPR-Cas9 for
831 study of immune function. *Immunity* **42**, 18-27 (2015).

59. E. Hemmila *et al.*, Ceacam1a-/- mice are completely resistant to infection by murine coronavirus mouse hepatitis virus A59. *J Virol* **78**, 10156-10165 (2004).
60. H. Zhou, S. Perlman, Mouse hepatitis virus does not induce Beta interferon synthesis and does not inhibit its induction by double-stranded RNA. *J Virol* **81**, 568-574 (2007).
61. X. Zhang, R. Goncalves, D. M. Mosser, The isolation and characterization of murine macrophages. *Curr Protoc Immunol* **Chapter 14**, 14 11 11-14 11 14 (2008).
62. A. R. Fehr *et al.*, The nsp3 macrodomain promotes virulence in mice with coronavirus-induced encephalitis. *J Virol* **89**, 1523-1536 (2015).
63. L. S. Voth *et al.*, Unique Mutations in the Murine Hepatitis Virus Macrodomain Differentially Attenuate Virus Replication, Indicating Multiple Roles for the Macrodomain in Coronavirus Replication. *J Virol* **95**, e0076621 (2021).
64. C. M. Kerr *et al.*, PARP12 is required to repress the replication of a Mac1 mutant coronavirus in a cell- and tissue-specific manner. *J Virol* **97**, e0088523 (2023).
65. W. Shi *et al.*, Isolation and purification of immune cells from the liver. *Int Immunopharmacol* **85**, 106632 (2020).

ACKNOWLEDGMENTS:

We thank the KU Flow Cytometry Core, KU Animal Care Unit, and all members of the Orozco lab for their discussions and assistance. We also thank Dr. Hans Dalton for his edits on this manuscript.

Funding Sources:

NIH T32 Chemical Biology T32 Training Grant GM13206 (AB)
KU Chemical Biology of Infectious Disease (COBRE) National Institute of General Medical Sciences (NIGMS) of the National Institutes of Health under award number P20GM113117 (RCO, ARF)
KU Center for Genomics Seed Grant (RCO)
Funds from the University of Kansas (RCO)
NIGMS R35GM138029 (ARF)
NIH T34 GM062232 (KJLHR)

Author contributions:

Conceptualization: AMB, ARF, RCO

Methodology: AMB, KJLHR, TC, CMK, SM, ARF, RCO

Investigation: AMB, KJLHR, NS, CMK, SM, RCO

Visualization: AMB, KJLHR, SM, ARF, RCO

Funding acquisition: AMB, KJLHR, SM???, RCO

Project administration: RCO

Supervision: SM, ARF, RCO

Writing – original draft: AMB, SM, ARF, RCO

Writing – review & editing: AMB, KJLHR, NS, TRC, CMK, SM, ARF, RCO

Competing interests:

Authors declare that they have no competing interests.

Data and materials availability:

All data are available in the main text or the supplementary materials. Raw data is available upon request.

Supplementary Materials

Fig. S1

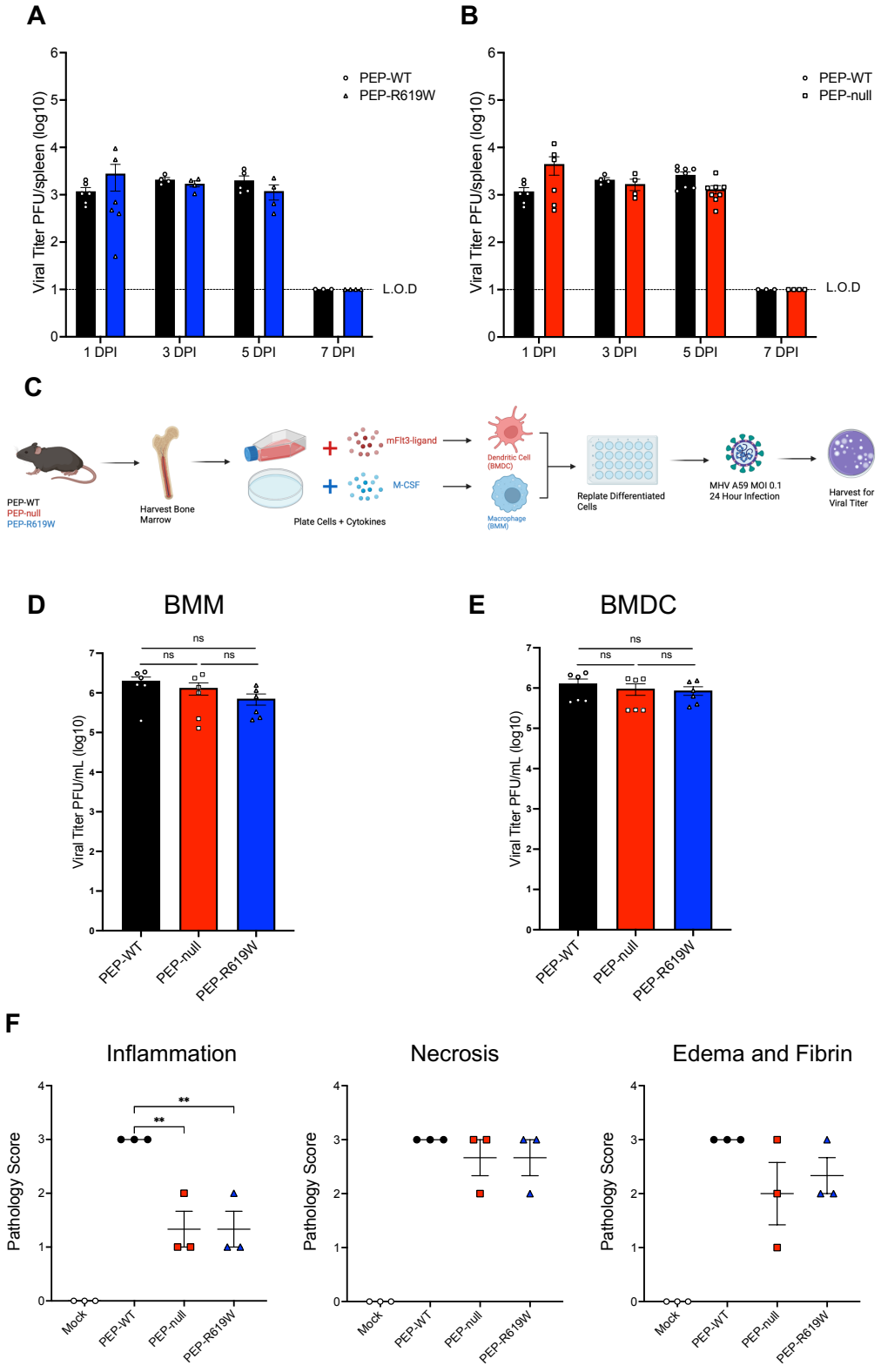

Figure S1: PEP-R619W does not impact splenic titer or restrict viral replication in myeloid cells.

To measure viral burden, spleen homogenates from infected (5e2 PFU MHV A59) PEP-WT, PEP-null, and PEP-R619W mice were used for plaque assay (A, B). Experimental schematic for deriving bone marrow-derived macrophages (BMMs) and bone marrow-derived dendritic cells (BMDCs) (C). The viral titer was quantified via Plaque Assay for BMMs (D) and BMDCs (E). Liver histopathology scores of individual parameters (inflammation, necrosis, and edema/fibrin) at 3 dpi following 1e5 PFU MHV A59 infection are shown (F). For whole spleen titer (A, B), each symbol represents an individual mouse. The dashed line indicates the limit of detection (L.O.D.). Certain PEP-WT mice are represented in both graphs, as some experiments had all three genotypes, whereas others contained only PEP-WT vs. PEP-null or PEP-R619W. Combined data from 2 independent experiments, multiple unpaired T-Tests, PEP-WT vs PEP-R619W, PEP-WT vs PEP-null, at each time point. For BMM and BMDC titer, each MHV A59 infection was performed at MOI = 0.1. Data are shown from two independent experiments with 3 technical replicates per experiment. For histopathological analysis, each dot represents an individual mouse, with p-values from One-way ANOVA with Tukey's Multiple Comparisons shown, *$p<0.05$, **$p<0.01$.

23 **Fig. S2**

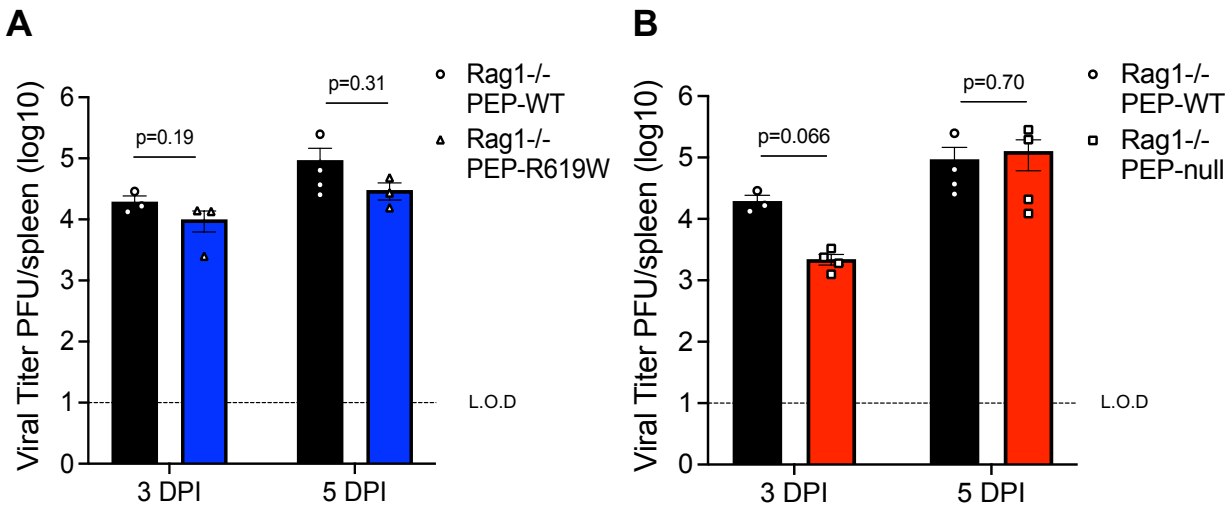

24 **Figure S2: Splenic titers are unchanged in Rag1-/- mice regardless of PEP**

25 **genotype.**

26 To measure viral burden, liver homogenates from infected (5e2 PFU) Rag1-/- PEP-

27 WT (black), Rag1-/- PEP-null (red), and Rag1-/- PEP-R619W (blue) mice were

28 used for plaque assay (A, B). Each symbol represents an individual mouse. The

29 dashed line indicates the limit of detection (L.O.D.). Certain Rag1-/- PEP-WT

30 mice are represented in both graphs, as some experiments had all three genotypes,

31 whereas others contained only Rag1-/- PEP-WT vs Rag1-/- PEP-null or Rag1-/-

32 PEP-R619W. Multiple unpaired T-Tests, PEP-WT vs PEP-R619W, PEP-WT vs

33 PEP-null, at each time point.

34 **Fig. S3**

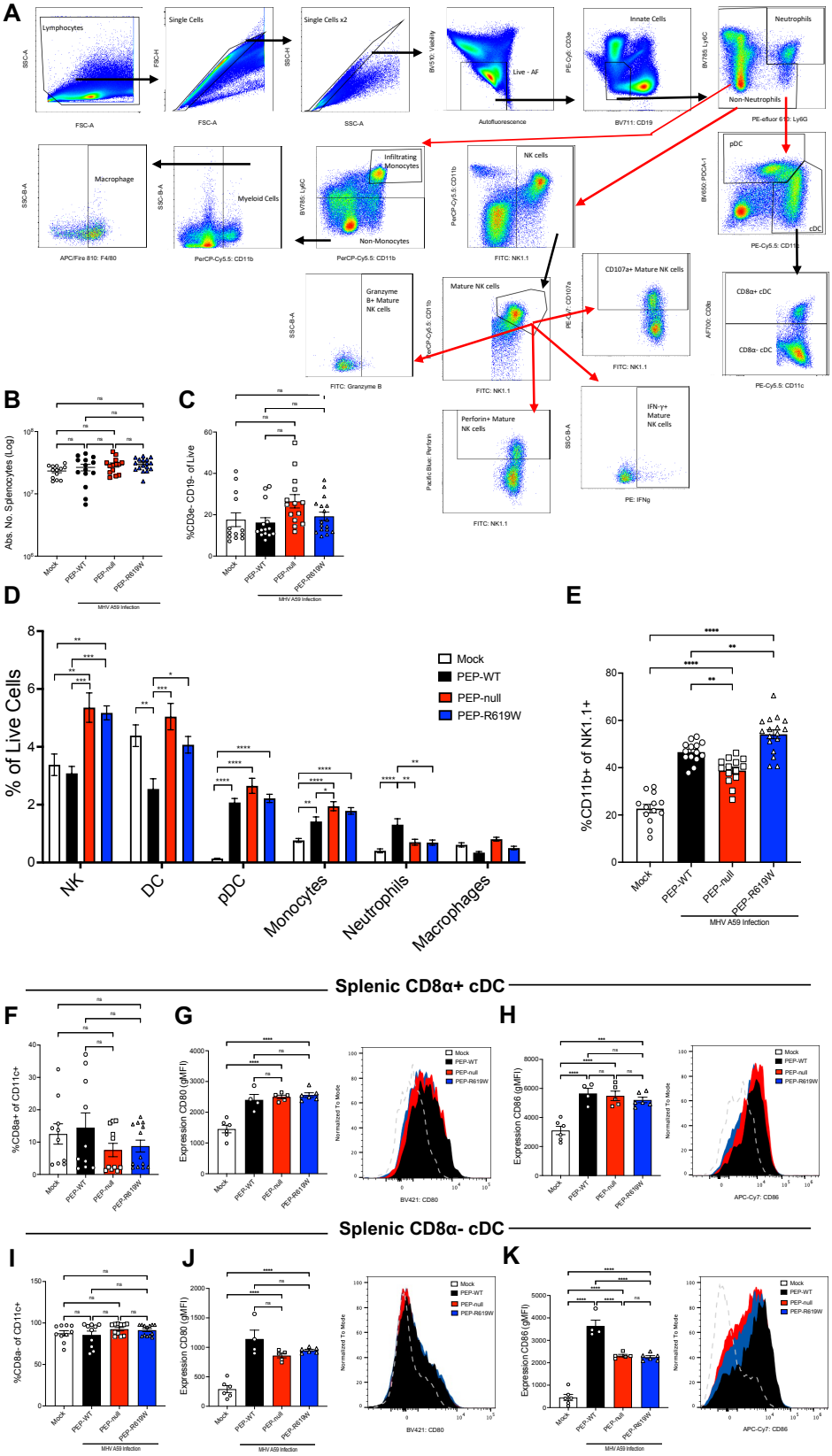
A
Lymphocytes
Single Cells
Single Cells x2
Live - AF
Innate Cells
Neutrophils
Non-Neutrophils
Macrophage
Myeloid Cells
Infiltrating Monocytes
Non-Monocytes
NK cells
pDC
cDC
Granzyme B+ Mature NK cells
Mature NK cells
CD107a+ Mature NK cells
CD8α+ cDC
CD8α- cDC
Perforin+ Mature NK cells
IFN-γ+ Mature NK cells
B
Abs. No. Splenocytes (Log)
C
%CD3e- CD19- of Live
D
% of Live Cells
Mock
PEP-WT
PEP-null
PEP-R619W
NK
DC
pDC
Monocytes
Neutrophils
Macrophages
E
%CD11b+ of NK1.1+
MHV A59 Infection
Splenic CD8α+ cDC
F
%CD8a+ of CD11c+
G
Expression CD80 (gMFI)
H
Expression CD86 (gMFI)
Splenic CD8α- cDC
I
%CD8a- of CD11c+
J
K

35 **Figure S3: PEP-R619W increases the splenic innate immune population.**
36 Representative gating strategies to identify splenic immune cell populations of
37 interest (A). Populations are labeled on flow cytometry plots, where black arrows
38 indicate the down-gating of the population from which they are drawn from, and
39 red arrows indicate the down-gating from one population to multiple populations.
40 Following PBS injection (Mock, white bar, circle) or 5e4 PFU MHV A59 infection
41 (i.p) in PEP-WT (black bar, circle), PEP-null (red bar, square), PEP-R619W (blue
42 bar, triangle) mice, at 3 dpi the spleen was harvested and antibody stained for flow
43 cytometric analysis. The absolute count of splenocytes for all genotypes (B).
44 Frequencies (%) of CD3e- CD19- of Live cells (C). Frequency (%) of several
45 innate cells of Live cells is shown (D). The gating strategy for all innate subsets is:
46 Lymphocytes> Single cell x2> autofluorescent-> Live> CD3e- CD19-> Ly6G-
47 Ly6C+/- (non-neutrophils). NK Cells: innate subsets> NK1.1+. DCs: innate
48 subsets> CD11c+ PDCA-1-. pDCs: innate subsets> PDCA-1+ CD11c+/-.
49 Monocytes: innate subsets> Ly6Chi CD11b+. Macrophage: innate subsets> Ly6C-
50 CD11b+/-> CD11b+> F4/80+. Neutrophils: Lymphocytes> Single cell x2>
51 autofluorescent-> Live> CD3e- CD19-> Ly6G+ Ly6C+. Frequency (%) of
52 CD11b+ (mature) NK cells (E). Frequency (%) Splenic CD8α+ cDCs (F) and
53 expression (gMFI) of CD80 (G) and CD86 (H) with representative histograms to
54 the right. Frequency (%) CD8α- cDCs (I) and expression (gMFI) of CD80 (J) and

55 CD86 (K) with representative histograms to the right. Quantification of flow
56 cytometric data was pooled from 3 independent experiments. Each symbol
57 represents an individual mouse. Mock mice are a mixture of all 3 genotypes. p-
58 values from One-way ANOVA with Tukey's Multiple Comparisons are shown for
59 each panel. *$p<0.05$, **$p<0.01$, ***$p<0.001$, ****$p<0.0001$.

Fig. S4

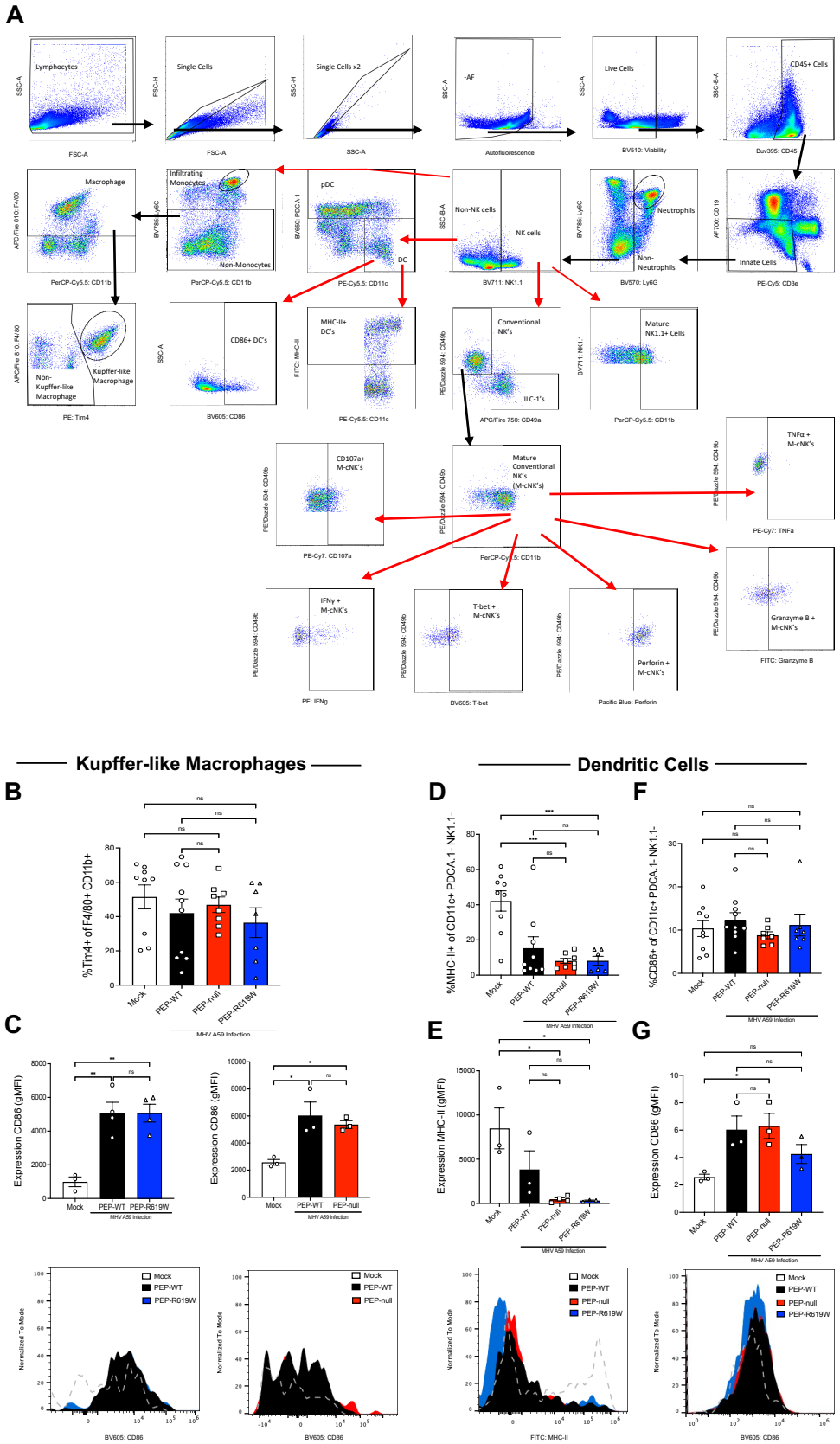
A
Lymphocytes
Single Cells
Single Cells x2
-AF
Live Cells
CD45+ Cells
Macrophage
Infiltrating Monocytes
Non-Monocytes
pDC
DC
Non-NK cells
NK cells
Neutrophils
Non-Neutrophils
Innate Cells
Non-Kupffer-like Macrophage
Kupffer-like Macrophage
CD86+ DC's
MHC-II+ DC's
Conventional NK's
ILC-1's
Mature NK1.1+ Cells
CD107a+ M-cNK's
Mature Conventional NK's (M-cNK's)
TNFα + M-cNK's
IFNγ + M-cNK's
T-bet + M-cNK's
Perforin + M-cNK's
Granzyme B + M-cNK's
Kupffer-like Macrophages
Dendritic Cells
B
%Tim4+ of F4/80+ CD11b+
C
Expression CD86 (gMFI)
D
%MHC-II+ of CD11c+ PDCA-1- NK1.1-
E
Expression MHC-II (gMFI)
F
%CD86+ of CD11c+ PDCA-1- NK1.1-
G
Mock
PEP-WT
PEP-null
PEP-R619W
MHV A59 Infection
Normalized To Mode

Figure S4: Representative gating strategy for different liver immune cell populations and additional quantification of immune cells.

Representative gating strategies to identify liver immune cell populations of interest presented in Figure 3 (A). Populations are labeled on flow cytometry plots, where black arrows indicate the down-gating of the population from which they are drawn from, and red arrows indicate the down-gating from one population to multiple populations. Following PBS injection (Mock, white bar, circle) or 1e5 PFU MHV A59 infection (i.p) in PEP-WT (black bar, circle), PEP-null (red bar, square), PEP-R619W (blue bar, triangle) mice, at 3 dpi the liver was perfused, harvested, and antibody stained for flow cytometric analysis. Tim4+ Macrophages (Kupffer-like cells) frequency (%) (B) and expression of CD86 (gMFI) in Tim4+ Macrophages (C), with representative histograms below. The first plot (left) comparing Mock, PEP-WT, and PEP-R619W and the second plot (right) comparing Mock, PEP-WT, and PEP-null are representative of two separate independent experiments. The gating strategy for Kupffer-like (Tim4+ macrophages) is: Lymphocytes> Single cell x2> autofluorescent-> Live> CD45+> CD3e- CD19-> Ly6G- Ly6C+/- (non-neutrophils)> NK1.1-> Ly6C- CD11b+/-> F4/80+ CD11b+> Tim4+. MHC-II+ DCs frequency (%) (D) and expression of MHC-II (gMFI) in DCs (E) with a representative histogram below. CD86+ DCs frequency (%) (F) and expression of CD86 (gMFI) in DCs (G) with a

81 representative histogram below. The gating strategy for MHC-II+ DCs or CD86+
82 DCs is: Lymphocytes> Single cell x2> autofluorescent-> Live> CD45+> CD3e-
83 CD19-> Ly6G- Ly6C+/- (non-neutrophils)> NK1.1-> CD11c+ PDCA-1-> MHC-
84 II+ or CD86+. Quantification of flow cytometric data was pooled from 2
85 independent experiments. Each symbol represents an individual mouse. Mock mice
86 are a mixture of all 3 genotypes. p-values from One-way ANOVA with Tukey's
87 Multiple Comparisons are shown for each panel. *$p<0.05$, **$p<0.01$, ***$p<0.001$,
88 ****$p<0.0001$.

89 **Fig. S5**

Mature NK Cell

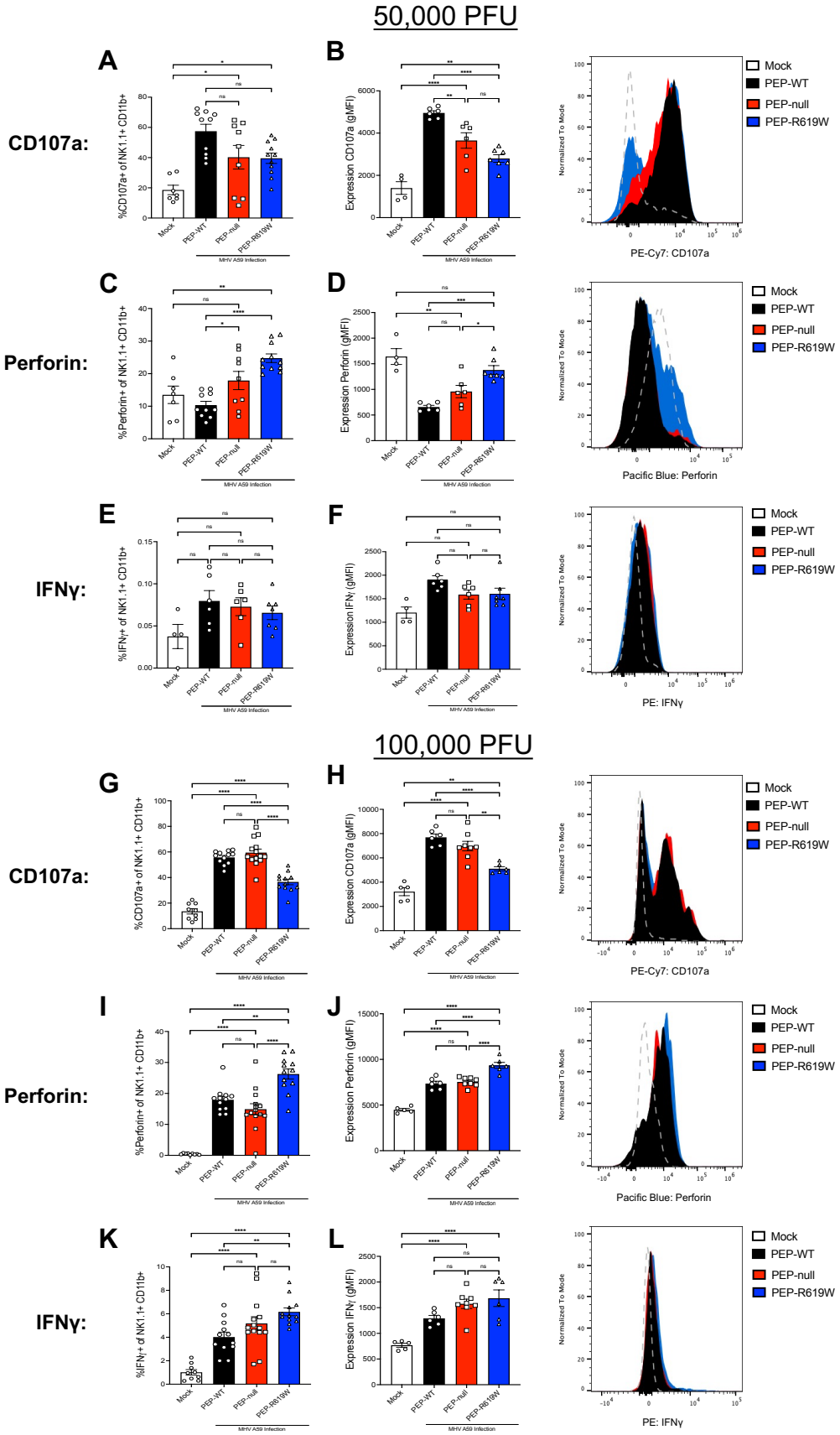

Figure S5: Infection dose-dependent impact on splenic mature NK function. Following PBS injection (Mock, white bar, circle) or 5e4 PFU (A-F) or 1e5 PFU (G-L) MHV A59 infection (i.p) in PEP-WT (black bar, circle), PEP-null (red bar, square), and PEP-R619W (blue bar, triangle) mice, at 3 dpi the spleen was harvested, surface and intracellularly antibody stained for flow cytometric analysis. Frequency (%), expression (gMFI), and representative histogram to the right of CD107a (A-B, G-H), Perforin (C-D, I-J), and IFNγ (E-F, K-L) in Mature NK cells, for 5e4 PFU and 1e5 PFU MHV A59 infections, respectively. The gating strategy for Mature NK cells and effector markers was: Lymphocytes> Single cell x2> autofluorescent-> Live> CD3e- CD19-> Ly6G- Ly6C+/- (non-neutrophils)> NK1.1+> CD11b+> CD107a+ or Perforin+ or IFNγ+. Frequencies of flow cytometric data are combined from 2 independent experiments, gMFI's are representative images from 2 independent experiments at each dose. Each symbol represents an individual mouse. Mock mice are a mixture of all 3 genotypes. p-values from One-way ANOVA with Tukey's Multiple Comparisons are shown for each panel. *$p<0.05$, **$p<0.01$, ***$p<0.001$, ****$p<0.0001$.

Fig. S6

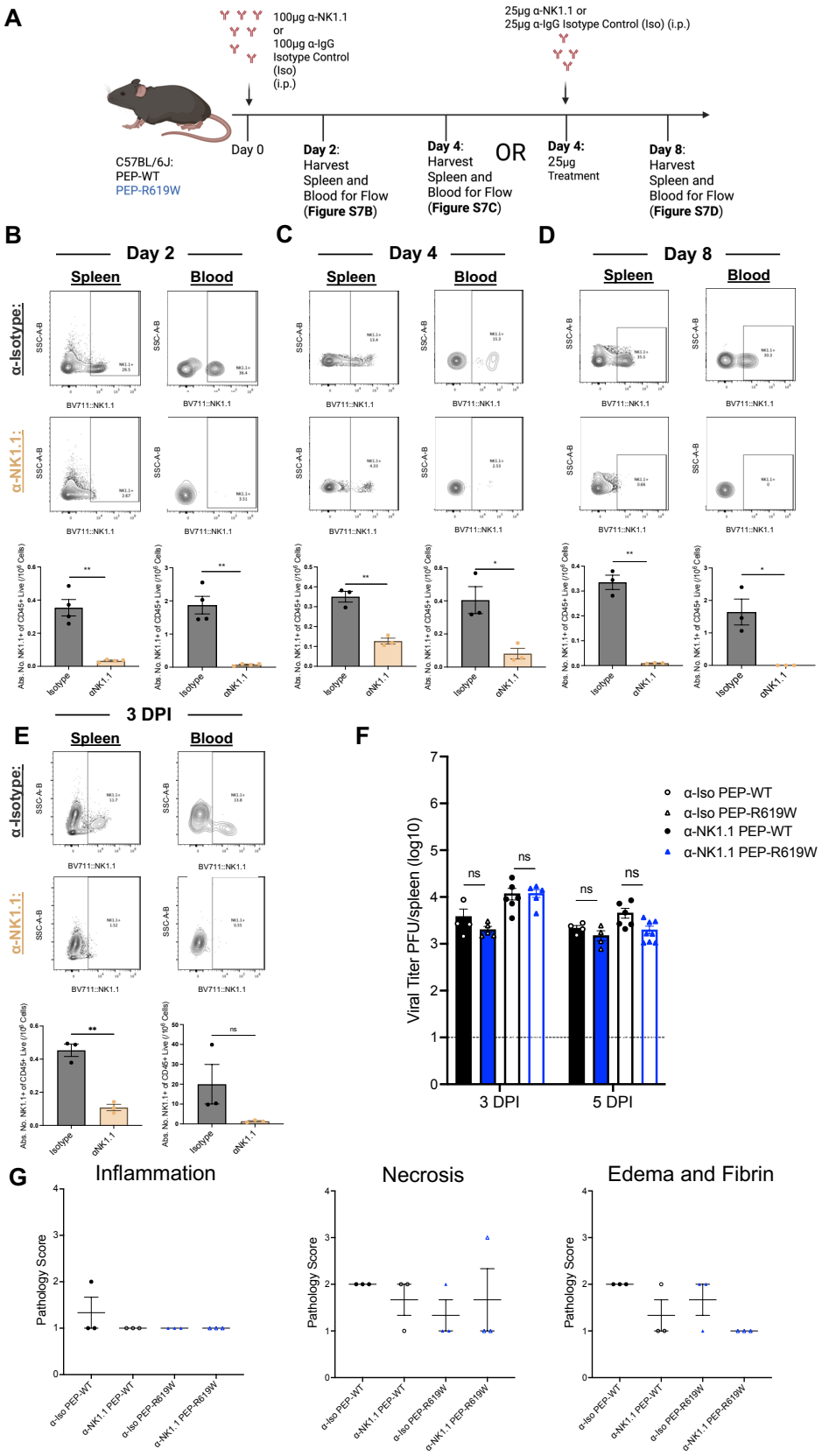
A
100µg α-NK1.1
or
100µg α-IgG
Isotype Control
(Iso)
(i.p.)
25µg α-NK1.1 or
25µg α-IgG Isotype Control (Iso) (i.p.)
C57BL/6J:
PEP-WT
PEP-R619W
Day 0
Day 2: Harvest Spleen and Blood for Flow (Figure S7B)
Day 4: Harvest Spleen and Blood for Flow (Figure S7C)
OR
Day 4: 25µg Treatment
Day 8: Harvest Spleen and Blood for Flow (Figure S7D)
B
Day 2
C
Day 4
D
Day 8
Spleen
Blood
α-Isotype:
α-NK1.1:
SSC-A-B
BV711::NK1.1
Isotype
αNK1.1
3 DPI
E
F
α-Iso PEP-WT
α-Iso PEP-R619W
α-NK1.1 PEP-WT
α-NK1.1 PEP-R619W
Viral Titer PFU/spleen (log10)
ns
3 DPI
5 DPI
G
Inflammation
Necrosis
Edema and Fibrin
Pathology Score
α-Iso PEP-WT
α-NK1.1 PEP-WT
α-Iso PEP-R619W
α-NK1.1 PEP-R619W

107 **Figure S6: NK depletion protocol and NK-depleted spleen titer and**

108 **histopathology scores.**

109 Experimental timeline detailing the concentration of α-NK1.1 antibody (Clone

110 PK136) and frequency of doses (A). NK cell depletion representative flow plots

111 and absolute counts of NK1.1+ cells (per 10^6 cells) are shown for the spleen and

112 peripheral blood at day 2 (B) and day 4 (C) post-100μg α-NK1.1 or α-Iso injection

113 (i.p). Alternatively, mice were administered 100μg α-NK1.1 or α-Iso injection (i.p),

114 and on day 4, an additional dose of 25μg α-NK1.1 or α-Iso injection was given.

115 NK cell depletion representative flow plots and absolute counts of NK1.1+ cells

116 (per 10^6 cells) are shown for the spleen and peripheral blood at day 8 (D). NK

117 depletion at 3 dpi following 1e5 PFU MHV A59 infection using the timeline

118 depicted in Figure 6A (E). Following 5e2 PFU MHV A59 infection (i.p), spleens

119 were harvested and tittered at the indicated days post-infection with NK depletion

120 (α-NK1.1) or non-depleting isotype control (α-Iso), with timeline depicted in

121 Figure 6A (F). Liver histopathology scores of individual parameters (inflammation,

122 necrosis and edema/fibrin) are shown (G). PEP-WT mice were used to verify NK

123 cell depletion. The gating strategy to identify splenic and peripheral blood NK cells

124 was: Lymphocytes> Single cell x2> autofluorescent-> Live> CD45+> CD3e-

125 CD19-> NK1.1+. Representative flow plots are shown from CD3e- CD19. Each

126 dot represents an individual mouse. p-values from Welch's unpaired t test are

127 shown for NK cell counts, *p<0.05, **p<0.01. Viral titers are pooled data from 2
128 independent experiments at each time point; comparisons are shown from multiple
129 unpaired T-Tests, α-Iso PEP-WT vs α-Iso PEP-R619W, α-NK1.1 PEP-WT vs α-
130 NK1.1 PEP-R619W. For histopathological analysis, each dot represents an
131 individual mouse, with p-values from One-way ANOVA with Tukey's Multiple
132 Comparisons shown, *p<0.05, **p<0.01.

133 **Table S1: Flow Cytometry Antibodies**

Antigen	Fluorophore	Dilution (1:x)	Company	Clone	CAT / REF	LOT
Ghost Viability	Violet510	1000	TONBO Biosciences	N/A	13-0870-T100	D0870120221133
CD45	Spark+ BUV395	200	BioLegend	30-F11	103192	B428503
CD45	BUV395	200	BD Biosciences	30-F11	564279	3205129
CD3e	PECy5	250	BioLegend	145-2C11	100309	B359890
CD19	BV711	400	BioLegend	6D5	115555	B287454
CD19	APC	250	BioLegend	6D5	115512	B371440
CD19	AF700	250	BioLegend	6D5	115512	B371440
Ly6C	BV785	400	BioLegend	HK1.4	128041	B386418
Ly6G	PE610	200	Invitrogen	1AB-Ly6g	61-9668-80	2445867
Ly6G	BV570	200	BioLegend	1AB	127629	B418454
CD11c	PECy5.5	200	Invitrogen	N418	35-0114-82	2286398
CD11c	APC-Cy7	200	BioLegend	N418	117324	B391502
CD8a	R710	200	TONBO Biosciences	53-6.7	80-0081-U100	C0081010722803
CD8a	AF700	200	BioLegend	53-6.7	100730	B401541
PDCA-1 (CD317)	Pacific Blue	200	BioLegend	927	127108	B302820
PDCA-1 (CD317)	BV421	200	BioLegend	927	127023	B365891
PDCA-1 (CD317)	BV650	200	BioLegend	927	127019	B365769
CD80	BV421	200	BioLegend	16-10A1	104725	B366741
CD86	APC/Cy7	200	BioLegend	GL-1	105029	B349514
CD86	BV605	200	BioLegend	GL-1	105037	B373866
F4/80	Pacific Orange	100	Invitrogen	BM8	MF48030	2209625
F4/80	PE	200	BioLegend	BM8	123109	B223149
F4/80	FITC	200	BioLegend	BM8	123108	B407719
F4/80	APC/Fire 810	200	BioLegend	BM8	123166	B431884
Tim4	PE	150	BioLegend	RMT4-54	130006	B428998
CD11b	PerCPCy5.5	200	TONBO Biosciences	M1/70	65-0112-U100	C0112121919653
CD11b	PerCPCy5.5	200	BioLegend	M1/70	101228	B423267
CD206	PEcy7	200	BioLegend	C068C2	141719	B239603
CD206	APC	150	Invitrogen	MR6F3	17-2061-80	1956852
MHC-II	FITC	150	BioLegend	M5/114.15.2	107606	B398140
NK1.1	FITC	200	BioLegend	PK136	108705	B376169
NK1.1	BV711	200	BioLegend	PK136	108745	B423146
CD49b	FITC	200	eBioscience	DX5	11-5971-82	E023186
CD49b	PE/Dazzle 594	200	BioLegend	DX5	108924	B396304
CD49b	PE	200	BioLegend	DX5	108908	B391901
CD49a	APC/Fire 750	200	BioLegend	HMα1	142610	B420608
CD107a	PEcy7	200	BioLegend	1D4B	121619	B348898
CD107a	BV650	200	BioLegend	1D4B	121645	B424309
CD27	BV605	200	BioLegend	LG.3A10	124249	B408891
CD27	AF700	200	BioLegend	LG.3A10	124240	B329641
IFNg	BV650	100	BioLegend	XMG1.2	505832	B361629
IFNg	PE	100	BioLegend	XMG1.2	505807	B366833
Perforin	Pacific Blue	100	BioLegend	S160009A	154311	B356368
Granzyme B	PE	100	Invitrogen	GB11	12-8899-41	2682463
Granzyme B	FITC	100	BioLegend	GB11	515403	B397296
TNFa	BV605	100	BioLegend	MP6-XT22	506329	B422381
TNFa	PE-Cy7	100	BioLegend	MP6-XT22	506324	B424713
T-bet	BV605	100	BioLegend	4B10	644817	B387805

134

135 List of antibodies used in various combinations throughout all experiments.

136 Antigen, fluorophore, dilution (1:x), company, clone, catalog/reference number,

137 and lot number listed.